THE RHEOLOGY OF HIGH ASPECT RATIO NANO-PARTICLE FILLED LIQUIDS

David W. Litchfield and Donald G. Baird

Virginia Tech Dept. of Chemical Engineering
& Macromolecules and Interfaces Institute
133 Randolph Hall Blacksburg, VA 24061, USA

ABSTRACT

The objective of this review is to elucidate the recent developments in the rheology of suspensions containing high aspect ratio (> 100) nano-scale fillers. In particular, this review focuses on industrially important nanoparticles, namely layered silicates or nanoclays, carbon nanotubes, and carbon nanofibers, suspended in low and high molecular weight liquids. This review begins with the critical aspects of nanoparticle structure. In addition, the surface chemistry is discussed in the context of particle-particle interactions leading to flocculation or aggregation, because optimum suspension properties occur in well-dispersed, non-aggregated systems. A comprehensive review of large aspect ratio nanoparticles in low and high molecular weight liquids is then presented, with discussions of the effects of particle size, surface treatment, meso-structural development on linear and non-linear viscoelastic properties (complex, steady shear, and extensional viscosity; shear thinning; stress overshoot; and primary normal stress difference where applicable). These sections elaborate on the following results of nanoparticle suspensions. First, nanocomposites require much lower concentrations for the same rheological effects as conventional micro-composites, because of the nanoparticle's larger available surface area and the development of a meso-structural polymer-nanoparticle network. Second, the linear viscoelastic properties generally increase with the addition of nanofiller, and the nanoparticles profoundly broaden the relaxation dynamics of the polymer melt. Third, the primary normal stress difference (N_1) becomes negative at high stresses and high nanoparticle loadings. Finally, nanoparticles increase the values of extensional viscosity as a function of Hencky strain to a greater extent than micron sized fillers. This review concludes with a discussion of recent theory concerning particle network development and the nature of particle-polymer interactions with an emphasis on what types of constitutive relations are needed to describe the rheology of fluids containing high aspect ratio nanoparticles.

KEYWORDS: Nanocomposite; rheology; viscoelasticity; normal stress; yield stress; extensional viscosity; layered silicates; carbon nanotubes; carbon nanofibers; colloidal suspensions.

1. INTRODUCTION TO NANOCOMPOSITE RHEOLOGY

In recent years there has been considerable interest in the use of nanoparticles to improve the mechanical, electrical, and barrier properties of polymers. Furthermore, nano-sized particles have been used as thickening agents for low viscosity Newtonian fluids. With the addition of nano-sized particles to fluids, it is desirable to know what their effect is on the rheology of the composite and what type of approach is needed to model the rheology of these systems. In addition, rheology may provide a means to determine the degree of exfoliation (i.e. degree of dispersion) of the nanoparticles in a polymer melt. Rheological properties of particulate suspensions are sensitive to structure, particle size and shape, and surface modification. Although most studies include forms of x-ray diffraction and/or electron micrographs to quantify and qualify nanoparticle dispersion, representations are made on a sampling basis and may differ from the bulk. Rheological properties change significantly with favorable particle-matrix interactions compared to non-interacting systems or strong particle-particle attractions. Thus, the study of the rheological properties of a nanocomposite system may yield an invaluable tool in structure characterization and property prediction, but the connection of structures to flow is not completely understood.

The addition of particles to a flowing liquid, with the complementary local disturbance of the flow lines, will result in the simplest flows becoming rather complicated. The flow pattern changes to a situation where locally in the liquid phase in the vicinity of the particle there is an increase and spatial variation of the shear rate in the continuous phase and transient behavior of local liquid elements. In the melt phase, the attractive van der Waals forces between particles encourage agglomeration and significantly influence flow properties from the increase in phase volume. Aggregated domains of nanoparticles increase the distortion of flow lines and have profound effects on rheological properties such as viscosity and normal stresses. Well-dispersed domains may be a result of favorable interaction between matrix and particle surfactant, such as the hydrogen bonding between hydroxyl modified nanosilicates and nylon polymers. At an equal particle concentration, exfoliated or well-dispersed nanoparticles exhibit different rheological behavior compared to their agglomerated counterparts. These complications invalidate any assumptions governing macroscopic homogeneity, forcing the application of complex constitutive equations over the heterogeneous phase to account for additional spatial and time derivatives as well as particle-particle and particle-matrix molecular interactions.

The complexity of filled liquids has created much scientific interest, especially in the rheological properties of particle suspensions on the nano-scale. Pieces of the available reviews of colloid suspensions and filled viscoelastic systems from some authors [1-10] provide some perspective but not the complete rheological picture of high aspect ratio nanoparticle suspensions. Such reviews have focused on spherical, near spherical or fibrous micron-sized particles, but as the particle size decreases and the particle shape elongates rheological behaviors begin to change, i.e. primary normal stress difference (N_1). The most recent review of nanoparticle rheology was completed as a chapter of layered-silicate polymer composite science by Ray and Okamoto [2] in 2003, and focused on 2-dimensional nanoclay particles in polymer matrices. Yet, a complete review of both shear and shear-free material functions for high aspect ratio

(1- and 2-D) nanoparticle suspensions in low molecular weight and polymeric liquids from both an experimental and a theoretical standpoint has yet to be accomplished and is the major aim of this work.

The following review of the observed phenomena in nanoparticle filled systems is presented in a format to cover the multitude of matrices and particles and their surface treatments discussed in the recent literature. The main body of text for a given rheological property covers the most prevalent filler type, nanosilicates, or platelet shaped particles including natural and synthetic clays for different matrices. Then the effects of carbon nanotubes and nanofiber are covered, as these fillers are the least abundant in the current literature. Covered under the filler types will be their effects on the rheological properties of the various types of polymer matrices and small molecule solvents. The most common thermoplastic matrices are polyamides, polyvinyls including polyolefins, polycarbonates, and polyesters. Aqueous suspensions are the most common in studies of nanoparticles suspended in mall molecule liquids. Yet thermosetting polymer nanocomposites begin as suspensions in low molecular weight organic liquids and are covered in sections entitled Newtonian precursors. Because the rheology is so dependent on the structure and properties of the particles, the inherent geometric and chemical structures of the most studied nanoparticles must be discussed first.

2. STRUCTURE AND PROPERTIES OF NANOPARTICLES

2.1 Nanoclays

To better understand the complex morphologies that occur in layered silicate nanocomposites, the structural details of the layered silicates, i.e. nanoclays, and their properties are briefly reviewed. The structure in figure 2.1, and for the nanoclays in this review, refers to a 2:1 phyllosilicate called montmorillonite (MMT). The structures of MMTs have two tetrahedral sheets surrounding a single octahedral sheet that form a single layer of 0.6 nm thickness. The tetrahedrons, pictured in figure 2.1, are composed of silicon-oxygen bonds that share a single oxygen bond with the octahedrons of aluminum- or magnesium-oxygen-hydroxyl bonds. In a real system six tetrahedrons form a hexagonally symmetric ring; the rendering in figure 2.1 has been flattened for simplicity. MMT has the generic formula of $M_y^+ nH_2O\left(Al_{2y}Mg_y\right)Si_4O_{10}\left(OH\right)_2$. For example, sodium montmorillonite, i.e. Na^+MMT, has the general chemical composition of $Na_{1/3}\left[\left(Al_{5/3}Mg_{1/3}\right)Si_4O_{10}\left(OH\right)_2\right]$. Tetrahedral ($Si^{4+}$) and octahedral ($Al^{3+}$ or Mg^{2+}) cations may be substituted by different valence ions to create a surface charge, which in the presence of water aids in the stacking layers together.

Layers are held together by van der Waals forces of attraction generated from charge balancing interlayer complexes. The inherent surface charge of the clay originates primarily from adsorption of ions through the silicate. For example, Si^{4+} is typically replaced by Al^{3+} or Fe^{3+} in the tetrahedral sheets, and Al^{3+} is substituted by Mg^{2+}, Fe^{2+}, or other cations in the octahedral sheets [1]. Yet, any smaller valence atom
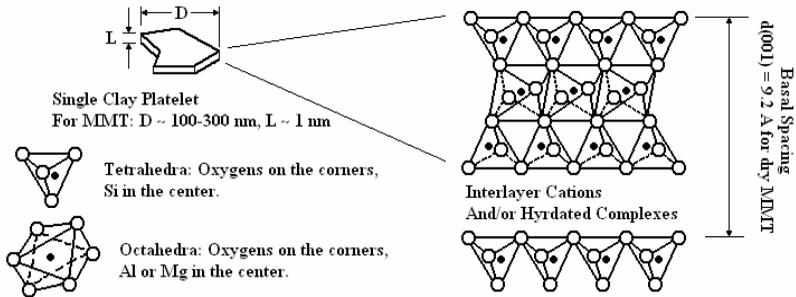
Figure 2.1: Schematic representation of layered silicates of the 2:1 phyllosilicate or smectite group. Lines are not scale representations of covalent bonds [117].

may replace a higher valence atom; for example tetrahedral Al may be substituted by K ions. For the clays of interest, the surface charge is naturally balanced by larger hydrated cationic complexes that adsorb on to the silicate surfaces and expand the interlayer distance. The amount of these interlayer cations is described in their unit of measure commonly called the charge exchange capacity (CEC) expressed in milliequivalents per 100g of dry clay. A reason for MMT's wide application in composites is its particularly high CEC (~ 90 mequiv/100g). Therefore, MMT is prone to cation exchange reactions that add surfactant molecules to improve particle-liquid interactions and, thus, the properties of the composite.

In general, the degree of dispersion of the clay platelets into the polymer matrix determines the super-structure of the nanocomposites. Depending on the interaction between the clay and the polymer matrix, two main idealized types of polymer-clay morphologies, intercalated and exfoliated, and a third less ideal flocculated morphology can be obtained (figure 2.2). Flocculation is more readily found in suspensions of charged particles in low viscosity, low molecular weight liquids, in which edge-edge interactions are significant. The intercalated structure results from penetration of a few polymer chains into the silicate interlayers. Face-to-face attractions persist resulting in formation of alternate layers of polymer and inorganic layers. The platelets are exfoliated when the individual silicate layers are completely separated and dispersed randomly in a polymer matrix, where no electrostatic interactions between surfaces exist. The best property improvements in polymer composites and the least influence to viscosity for low molecular weight suspensions results from the exfoliated morphologies.
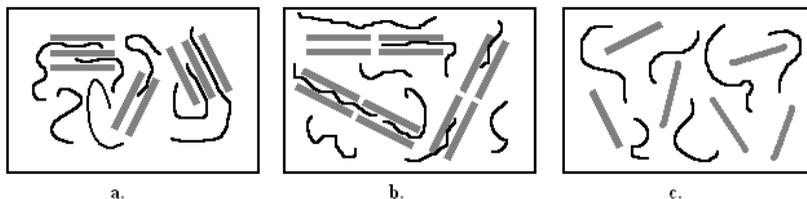
Figure 2.2: Schematic illustrations of two types of polymer-layered silicate morphologies: (a) intercalated, (b) flocculated edge-edge interactions between platelets, and (c) exfoliated [105].

2.2 Carbon Nanotubes (CNT) and Nanofibers (CNF)

Carbon nanotubes (CNTs) are cylindrically shaped carbon molecules with properties that make them useful in electronics, optics, and materials applications. The exceptional mechanical and transport properties of CNTs provide useful insight into the potential for nanoparticle additives in liquids and solid polymers to achieve significant improvements in bulk properties at low volume concentrations. The uniqueness of CNT properties arises from the structure and molecular arrangement of the carbon atoms.

Single-walled nanotubes have diameters close to 1nm, with a length that can possibly reach the millimeter scale. The structure of a single-walled nanotube is composed of a seamless wrap of a single nanometer thick graphene sheet. The graphene sheet wraps into a cylinder characterized by two integer indices (n,m) to form a chiral vector normal to the tube axis. The wrapping structure or orientation of the chiral vector dictates the electronic properties of the tube. Any "metallic" nanotube (for which (n-m)/3 = integer) has a current density 1,000 times stronger than copper [11]. Otherwise, the remaining nanotube population is semi-conductive. Yet, the tensile properties of single-walled and multi-walled nanotubes are weak functions of the chiral vector. For single-walled nanotubes the tensile strength is an order of magnitude greater than steel and the elastic modulus is in the tera-Pascal range (10^{12} Pa) [12].

Multi-walled nanotubes are composed of repeated sheaths, or cylinders within cylinders, of single-walled nanotubes. Multi-walled nanotubes have diameters on the order of tens of nanometers with length ranges in the thousands of nanometers. Typically the reported properties are lower than their single-walled constituents because of the increased probability of critical defects. An abundance of defects often produces tensile properties two or three orders of magnitude lower than their more perfect counter parts. A review by Hidling [13] provides a detailed comparison of

calculated versus experimental mechanical and transport properties of single- and multi- walled nanotubes.

The method of nanotube synthesis will dictate the formation and concentration of single- or multi-walled nanotubes, as well as the morphology of the CNT product. Chemical vapor deposition [14], electric arc discharge [15], and solid pyrolysis [16] are among the documented processes used in CNT formation. Aspect ratio, purity, defects, and degree of physical or chemical entanglements depend on the CNT synthesis method and significantly effect melt rheology. Until nanotube manufacturing yields CNTs suitable for direct end applications, nanotube ropes must be dispersed or exfoliated within a given matrix or substrate for further processing. Formation of CNT aggregates prevents efficient distribution of mechanical loads and isotropic transport coefficients by reducing interaction between the polymer and nanotube. However, entangled aggregates can be difficult to disperse without causing fragmentation and reducing the aspect ratio. In the un-entangled state, the high aspect ratio leads to physical contacts between particles in the fluids creating a network to improve thermal and electrical conductivity of the composite. In addition to increasing tensile and mechanical properties, the viscosity of suspensions of such high aspect ratio nanoparticles increases. Understanding the rheology of these filled materials will shed light on the composite properties after processing in unit operations necessary for large-scale production. For now and the near future, the use of CNTs is confined to high-end engineering applications and research interests because of their high cost.

Carbon nanofibers (CNF) possess similar chemical composition to nanotubes and present a cheaper alternative without sacrificing the majority of attractive mechanical and transport properties in composite form. One method of CNF preparation is the chemical deposition of ethylene gas on a copper catalyst to produce vapor grown nanofibers [17]. A CNF can be visualized as a thick single-walled nanotube, in which the center may be hollow, but carbon atoms are bonded in the radial direction. Reported CNF diameters range from 50-200 nm with lengths ranging from 20-100 µm [18]. Like nanotubes, purification and functionalization processes are required to remove by-products and to disperse the highly entangled nanofibers without truncating the aspect ratio by shortening the fiber length. Solvent casting or melt blending are two convenient methods for dispersion of nanofibers in polymeric matrices. Solvent casting methods, such as ultra-sonication in an appropriate solvent and dissolved polymer, disperse the nanofiber with less truncation of fiber ends than melt compounding in a polymer matrix under high shear [18]. The advantage of a larger aspect ratio provides greater probability of nanofiber contacts with the suspending matrix, which leads to greater improvements of composite properties over a lower aspect ratio, or more agglomerated nanofiber filler. Nevertheless, CNFs can be produced in large quantities and are relatively inexpensive, which are two factors propelling their interest in current research.

2.3 Particle Surface Treatments

A common observation in nanocomposite rheology is that flocculated or agglomerated particles produce larger viscosity increases than well-dispersed or

exfoliated systems of equal particle loading. Therefore, one may state that flocculation or agglomeration artificially increases particle concentration. Thus, to optimize mechanical property improvements, the particles (platelets, tubes, or spheres) must be exfoliated. This task is not easily accomplished because the particle surfaces and suspending liquid may have unmatched chemical affinity. For example, layered-silicates are naturally hydrophilic, and do not interact favorably with a non-polar, polypropylene, matrix. Nevertheless, such obstacles are overcome with the addition of ionic and/or organic compounds to more effectively wet the particle surfaces.

In terms of clay composites, exfoliation of the platelets in low molecular weight liquids depends on the electric double layer thickness of the platelet faces, whereas polymer suspensions require larger steric hindrances between plates. At low salt (or organic anions) concentrations (and depending of pH for aqueous systems), the compression of the electric double layer repulses other clay platelets and promotes exfoliation. Highly adsorbed polyelectrolytes and non-ionic polymers on clay surfaces provide an "entropic" repulsion due to the steric barrier that the dangling ends provide [1]. For polymer suspensions, cationic quaternary alkyl ammonium salts (or bases) are the most used surfactants, because the compounds strongly adsorb to the platelet surfaces, displacing interlayer water and increasing basal spacings to allow for easier polymer chain intercalation [19,20]. Different groups may be added to the amine to improve polymer-clay interactions, such as hydroxyls to promote hydrogen bonding.

For nanotube suspensions, acid treatments leave functional sites that promote dispersion in polar solvents, but shorten tube/fiber lengths. Surfactants, such as sodium dodecyl benzene sulfonate [21], surround the tube surface in long alkyl tails headed by hydrophilic sulfonate anions that increase aqueous interactions and provide enough steric hindrance to prevent aggregation, or roping, of single-walled nanotubes. Islam et al. [21] were able to disperse up to 65% nanotubes into single tubes of 1 nm diameter using dodecyl benzyl sulfonate among other less effective surfactants.

2.4 Other Nanoparticles

Novel nanoparticles are continually being developed by researchers but, to limit the scope of this review, the focus lies on the high aspect ratio particles discussed above because these structures are of immense industrial and academic interest. Yet, other nanoparticles that could be considered as significant but that are not discussed are listed below. Low aspect ratio, carbon fullerenes have been found to be suspendible in a number of small molecule liquids but only in dilute concentrations. At these solubility limits, the particles do not influence the elastic properties of the fluid [22], and higher concentrations of particles precipitate creating an inhomogeneous mixture. For these reasons, fullerene applications involve drug delivery and high performance solid lubricants [23-27], but not as polymer composites. As an interesting alternative to fullerenes, crosslinked polymer particles of nano-scale diameters that are mixed with linear chains of the same polymer demonstrate some unusual rheology. The particles are synthesized by a method of intra-molecular collapse, in which functional groups on originally linear polymer chains chemically bond to form a 3-dimensional nanoparticle [28]. These particles are becoming realized as ideal for

computational thermodynamic simulations, because of the absence of enthalpy restrictions. Calcium carbonate and titanium oxide particles possess large specific surface energies and strongly agglomerate to produce broad size distributions. Therefore, these particles are traditionally considered as having low aspect ratios and near spherical geometries. In terms of other high aspect ratio nanoparticles, inorganic nanotubes of tungsten sulfide, molybdenum sulfide, etc. are nanoparticles that have been studied in dispersed situations but omitted because scientific applications have been limited to solid tribology and atomic imaging [29].

3. RHEOLOGY OF NANOPARTICLE SUSPENSIONS IN LOW MOLECULAR WEIGHT LIQUIDS

Attention from industry on nanoparticle solutions has stemmed from past interest in the viscosity thickening properties of particle suspensions. The simplest cases arise from nanoparticles suspended in mediums of constant viscosity. Yet, these suspensions are far from being completely understood, as factors such as particle size distribution, volume fraction, and charge influence rheological behaviors. The properties of the medium, such as pH, polarity, and inherent functionality, also dictate flow behavior by regulating the degree of flocculation or aggregation. There are other factors that can influence results, for example the plate roughness or vane geometry of the testing device, which dictates the degree of slip at the wall and the amount of phase separation due to gravity or poor liquid-particle interactions.

The general trend in viscosity, as a function of particle concentration, has been semi-empirically modeled by several authors [30-35]:

$$\eta_{sp} = \eta_r - 1 = \eta/\eta_s - 1 = 2.5\phi \qquad \qquad ....(1)$$

$$\frac{\eta}{\eta_s} = 1 + 2.5\phi + 6.2\phi^2 \qquad \qquad ....(2)$$

$$\frac{\eta}{\eta_s} = \left(1 - k\phi\right)^x \qquad \qquad ....(3)$$

$$\frac{\eta}{\eta_s} = \left(\frac{1}{1 - \phi/\phi_m}\right)^{\phi_m[\eta]} \qquad \qquad ....(4)$$

The analysis began with Einstein's early 20th century relation (equation (1)) and has since been developed by Baker and later authors to include non-spherical geometries and shear thinning continuous phases [7]. The more often applied, semi-empirical models for high aspect ratio particles in suspension are of the type in equation (3), in which a common analogue is the Krieger Dougherty equation (4). Most analyses include a comparison to the hydrodynamically based Einstein equation of the form in equation (2), referred to as the Einstein-Batchelor equation. Such comparisons usually favor the Baker type equations because of the onset of shear thinning in more concentrated suspensions. At high particle loadings the Einstein type

equations perform expectedly poor, although their parameters are more straightforward than those of Baker. For example, the equation of Krieger and Dougherty [33] requires a maximum packing volume fraction, ϕ_m, of the particulate and an intrinsic viscosity parameter, $[\eta]$, to empirically model the effect of particle concentration on the suspension viscosity. The effects of particle size distribution are carried into ϕ_m, and the effects of shear thinning are absorbed into the $[\eta]$ term. Xu and coworkers [36] studied the effect of aspect ratio on the relative viscosity of CNFs in glycerol and water. Figure 3.1 shows the Krieger-Dougherty equation fitted their data well at high concentrations of filler, contrary to the Einstein-Batchelor equation. The authors examined a high and low aspect ratio CNF suspension and determined as the aspect ratio increases, the maximum packing fraction decreases. As a comparison, a suspension of 30x700 µm glass rods, the maximum packing fraction was $\phi_m = 0.27$ [37]; yet, for a suspension of non-interacting CNFs, $\phi_m = 0.05$ [36].

However, these semi-empirical models do not account for particle interactions or particle alignment under shear. Attempts can be made to place particle-particle interactions into the maximum packing factor, because particles typically agglomerate to increase the effective particle size. Yet, particle-liquid interactions combined with particle-particle interactions generate flocculates and aggregates that are formed and broken down during flow. Thus, the effective volume fraction could change as a function shear rate. In addition, high aspect ratio particles align in the direction of flow, and, therefore, the maximum packing factor increases as the particles align.
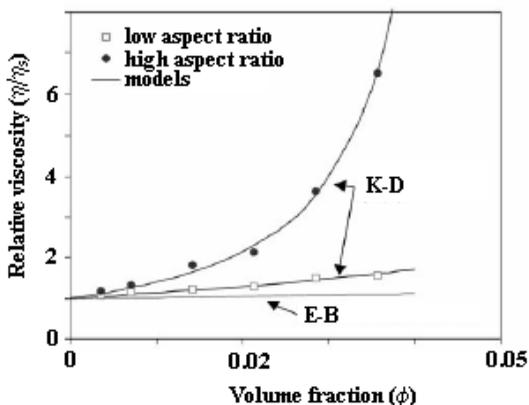

Figure 3.1: The effect of CNF concentration on the relative viscosity of 90% glycerol/water and the prediction accuracy of the semi-empirical Kreiger-Dougherty (K-D) equation over the hydrodynamic based Einstein-Bachelor (E-B) equation [36].

3.1 Layered-Silicate Suspensions

For dilute sols and suspensions, where the concentration of clay is so low that the platelets are non-interacting, the behavior is Newtonian. Einstein derived an equation for the viscosity increase from non-interacting spherical solids in suspension (see equation 1 above). However, for large aspect ratio, anisometric, platelets a larger proportionality constant is warranted. Van Olphen [1] suggested for large thin disks with small height to diameter ratios:

$$\eta_{sp} = 32\phi/(15\pi p) ; \hspace{4cm} ....(5)$$

$$\phi = m_c/(2.85(100-a)) , \hspace{3.5cm} ....(6)$$

where p is the aspect ratio, m_c is the mass in grams of dry clay per 100 cm^3 of suspension, 2.85 g/cm^3 is the density of dry clay, and a is the volume percent of water in the expanded clay derived from hydration basal spacings. Thus, according to theory, for dilute suspensions only the volume of clay influences the rheological response, not the number of platelets or degree of agglomeration. Kislenko and Verlinskaya [38] observed that agglomerated nanoclay suspensions behave as featureless Newtonian liquids.

For this section only the rheology of Na$^+$ MMT suspensions are discussed in detail. Although rheological experiments have been conducted on other types of clay suspensions such as illitites and kaolinites, the smectite clays, especially Na$^+$ MMTs, show the best swelling behavior [1, 39-41]. An inherent swelling ability is energetically favored in particle exfoliation, as larger swelling creates greater interlayer distances. Additionally, for aqueous suspensions of MMT, the presence of yield stress has been directly related to Na$^+$ ion concentration, because of sodium's ability to form strongly hydrated complexes within the interlayer spacing [42].

Exfoliated nanoclay filled liquids typically exhibit a non-Newtonian yield stress above the percolation limit and, hence, the gel phase is of prevalent interest in the recent literature. The yield behavior is related to the mesostructure of the suspension, in which the applied stress can result in a sol-gel transition to change the structure of the suspension from a solid to a flowing liquid over time in a narrow stress range. In a study of organically modified montmorillonite clay and xylene, the yield stress, which was determined by creep testing of clay suspensions containing clay weights from 1-6%, was found to increase rapidly with concentration [43]. The yield stress and critical shear are measures of the degree of particle association and are indicators of changes in inter-particle interaction modes [44]. The breakdown of particle-particle interactions is a result of shear or hydrodynamic forces, but the time-dependent buildup of particle interactions leading to yield stress values is solely related to Brownian motion as the particles collide with each other.

Studies on creep compliance of nanoclay solutions have attempted to elucidate the mechanism network reformation. Zhong and Wang [43] scaled the viscosity to the volume fraction of clay as $\eta \sim \phi^3$ and the equilibrium creep compliance as $J_e^\circ \sim \phi^{-3}$, implying that relaxation is nearly constant with respect to clay concentration, as shown in figure 3.2. The retardation time or lifetime of network entanglements is observed to be nearly constant for clay loading greater than 3 wt%, such that the increased number
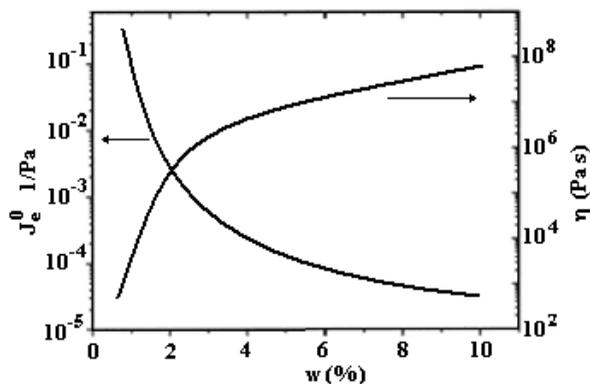
Figure 3.2: Schematic of creep and recovery results of a 4 wt% nanoclay suspension from Zong and Wang [43]. The curves show creep compliance and viscosity of suspension as a function of silicate loading. The nanoclay modifier used in this case is dehydrogenated tallow quaternarty ammonium chloride.

of entanglements from higher clay concentrations leads to higher viscosities. The authors proposed that nano-confinement of liquid xylene between the clay platelets increases the solid volume and leads to elastic solid-like response. Time dependent studies have shown that higher concentrations of clay slow the kinetics of quiescent structure recovery [43, 45]. Yet, as figure 3.2 implies, the relaxation is unaffected.

The addition of electrolytes to a suspension of clay platelets influences the double layer thickness, which dictates the mechanism of particle association. The addition of sodium hydroxide in low concentrations lowers an unmodified clay/water solution viscosity, suggesting the electrolyte weakens attractive forces between clay surfaces and the clay platelets are aligned along their positive ends. At high concentrations the apparent viscosity increases as the repulsion energy is reduced and clay platelets interact face to face to confine the solvent in tighter spaces producing a more solid-like response [44]. Additionally, at high salt concentrations the yield stress was reduced due to the decrease in network links from increased platelet agglomeration. Maino and Rabaioli [46] observed a transition from edge-face to face-face platelet interactions with increasing salt loading. Yet others [47] have shown that particles associate only edge-to-edge or face-to-face.

Pignon et al. [48] explored the mesostructural aspects of nanoclay/water suspensions of weak electrolyte concentration in a coupled rheological and light scattering study. The authors suggested a fractal arrangement of nanometric units of
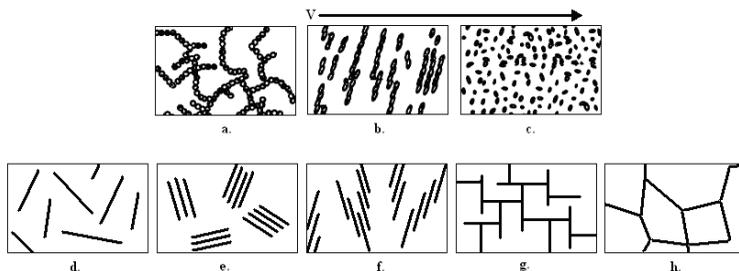
Figure 3.3: Schematic of nanoclay platelet mesostructures adapted from Pignon et al [48] and Luckham and Rossi [5]:

> a – the percolation of platelet clusters under rest;
> b – upon deformation rodlike aggregates form along the direction of the velocity gradient;
> c – under further deformation the aggregates break up into individual clusters;
> d – exfoliated platelets;
> e – face-to-face aggregates;
> f – face-to-face "band-like" aggregates to form a network;
> g – edge-to-face percolated network;
> h – edge-to-edge "house of cards" percolated network structure.

clay that extend to the tens of nanometers and form larger micrometer sized agglomerates at rest (for example, see figure 3.3). The sol-gel transition of their laponite clay and water system was about 0.5 vol %. Typical micron sized particles begin to form gels at much higher volume fractions, which were usually in the 20-50 vol % range. Yet, under shear, the fibrous structure of the isotropic phase was broken into rod-like aggregates perpendicular to the flow direction, which in turn they dispersed into micrometer flocculations upon longer or stronger deformation.

This interpretation was built on observations from previous authors [49-51]. Pignon and coworkers noted that as the shear rate increased, the dispersion of clay concentration increased to suggest the breakup of larger rod-like aggregates of flocs to smaller moieties. The proposed mechanism of network deformation of nanoclay/water suspensions suggested two time scales for the breakdown of structure. During the first few moments of shear the nanoclay aggregates oriented perpendicular to flow until the peak stress in the material was exceeded, depicted in figure 3.3(a-c). The long time scale of dis-aggregation and elimination of fractal characteristics began after the critical strain was exceeded. Then during the recovery under quiescence, the anisotropic disks orient to collective aggregates followed by a deformation history

dependent rearrangement to a fractal structure. This structure was marked by a time dependent increase in viscoelastic moduli, which under due time gave an equal behavior to the original gel.

The discussion so far has mainly pertained to charge stabilization, yet steric stabilization by polymer surfactants dictates rheological response. Ionic steric stabilizers, such as the popular quaternary ammonium salts or bases ($R_4N^+Cl^-$ or $R_4N^+OH^-$), substitute the interlayer cations and displace water to form a diffuse double layer of non-polar chains, which makes the clay suspensions stable in non-polar solvents. The discussions of Zhong and Wang [43] above involved an alkyl-ammonium quaternary cation to stabilize MMT in xylene. Non-ionic steric stabilizers are typically low molecular weight polymers that loop on, train along, and dangle off platelet surfaces and prevent agglomeration by reducing van der Waals forces between faces. In very dilute suspensions of Na^+MMT in polyethylene glycol (PEG) the viscosity was shown to decrease with increasing polymer concentration until a minimum, at which the de-flocculated particles, now arranged face-to-face, adsorb more polymer surfactant ultimately bridging platelets together [52]. In more concentrated silica/PEG suspensions the viscosity increased with polymer concentration until a maximum, at which the number of bridges between particles was reduced as the PEG polymer filled the available interactive sites on platelet surface [53, 54]. As expected the apparent yield stress reached a maximum of a critical polymer concentration due to the rising number of bridges. These bridges acted as effective gel points that trap solvent molecules and produce a more solid-like response until the saturation. At this point progressive micelles began to form and induced the deterioration of the network structure.

3.2 Thermosetting Layered-Silicate Nanocomposites, Newtonian Precursors

The majority of thermoset-layered silicate research has focused on epoxy-based precursors, which by themselves are Newtonian fluids. Similar to their non-reactive analogues, the control of exfoliation for epoxy suspensions depends upon the nanoparticle composition, the curing rate, and the compatibility of the two phases. Processing variables such as temperature and initial dispersion play an important role in the formation epoxy composites. An increase in temperature lowers the viscosity to improve the interlayer diffusion of monomer within the platelets and upon cure aids in delamination producing exfoliated thermoset composites. The addition of modified montmorillonite increases dynamic viscosity values with increasing clay content in an uncured epoxy monomer. The viscosity versus angular frequency curve reflects similar shear thinning behavior of particulate suspensions and weakly agglomerated gels, where larger contents of clay produce steeper shear thinning regimes.

As mentioned before, the epoxy nanoclay compatibility influences the degree of viscosity enhancement. Brown et al [55] compared the degree of exfoliation of hydroxyl modified silicate to a long alkyl chain or tallow modified silicate. The authors found that not only were the hydroxyl-modified clays exfoliated in the final cured matrix, and the tallow-modified clays intercalated, but that the surface modification influenced the kinetics of the curing time. At equal concentrations of clay
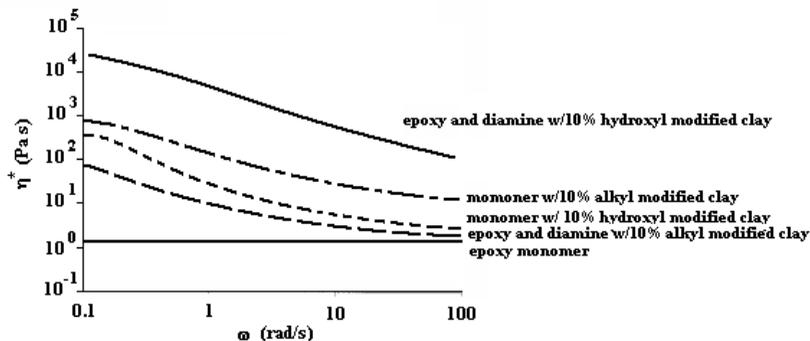
Figure 3.4: Complex viscosity of a 10 wt% nanoclay/epoxy suspension showing the significant effect surface treatment on favorable interactions [55].

loading, the larger magnitude of viscosity, for an alkyl modified clay over an hydroxyl modification, was attributed to the formation of larger aggregates, which occlude more liquid between the platelet surfaces. Smaller aggregate sizes showed smaller increases in the magnitude of viscosity. The subsequent addition of diamine to crosslink and form the final matrix had little effect on shear thinning characteristics of either clay modifier, but the ability of the hydroxyl modified clay to hydrogen bond to the hydroxyl-amine group produced a 2-3 order of magnitude upward shift in viscosity [55]. The tallow-modified clay showed little interaction with the crosslinking agent and marginally increased the viscosity, as shown in fig 3.4.

In recent articles, the time-dependent shear rheology of organically modified layer-silicate and epoxy nanocomposites was examined. Dean et al. [56] conducted time sweeps of dynamic moduli that showed the expected behavior of slowly rising storage, G', and loss moduli, G'', followed by a steep increase as the gel point was reached and then a flattening out to final properties as the composite vitrified. Their gel time decreased with increasing hydroxyl-modified clay content. The authors found that the balance between solution and particle polarity dictated the strength of inter-particle forces and the length of platelet separation available for diffusion of crosslinking agent. Similar results were obtained by le Pluart et al. [57], who built on the work of Moraru [58], to extend the observations of particle-solvent pairing to epoxy precursors. At equal clay concentrations, good organic modifier-solvent interactions produced weak gels with thixotropic behavior, whereas poor interactions produced strong gels with characteristic Newtonian behavior due to aggregate formation [57].

3.3 Nano-Fibrous Suspensions

The application of CNT and CNF reinforced composites share potential in the electronics industry as well as engineering materials in general. Processing nanotube or nanofiber suspensions must be understood to produce optimal properties. The addition of CNTs of CNFs to Newtonian liquids leads to non-Newtonian behavior strictly as an effect of the presence of filler. Therefore, the study of nanotube and nanofiber suspensions in small molecule liquids can be extended to more complex polymeric nanocomposites. Only a small volume fraction of nanotubes added to a Newtonian liquid is enough to dramatically change the rheological properties. Typical non-Newtonian behaviors, such as yield stress and shear thinning, have been shown to occur at volume fractions less than 1% [59]. Similar to other particles in suspension, the percolation threshold and rheological response (for example, onset and degree of shear thinning) are functions of nanotube orientation, aspect ratio, concentration, and even surface treatment [59, 60]. Advani and Fan [60] have recently discussed the effect of such variables for single-walled CNTs in epoxy suspensions.

Hough and coworkers [59] have achieved some success in effectively dispersing single-walled CNTs in water using a surface treatment, which produced aggregates no larger than 10 nm in diameter and a percolation volume fraction of 0.0026. Of the dynamic responses probed, the increased storage modulus, shown in figure 3.5, for these suspensions at low frequency was due to the formation and strengthening of a percolated network of physical, freely rotating nanotube-nanotube
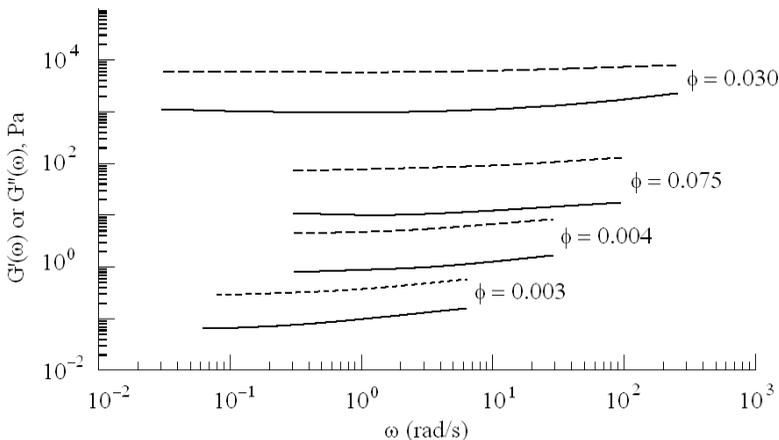

Figure 3.5: Storage and Loss Moduli as a function of angular frequency at 1% strain and for various CNT loadings, adapted from [59] Dashed lines – G'', solid lines – G'.

interactions. At a strain amplitude greater than 1% strain thinning occurs; as such $G'' > G'$, depending on the CNT concentration. Hough et al. contrasted their nanotubes against actin suspensions [61] that flex and stretch, rather than bond together, to increase G' with concentration. At large strains liquid-like behavior exceeded the initial solid like response ($G'' > G'$) and suggested that the nanotube rods underwent rotations from their major axis to debond and disentangle from their nearest neighbors, and therefore the enhancement of G' is not due to flexing or stretching of the nanotube particles. Hough et al. also showed success in developing a model for the yield stress, based on arguments of Doi-Edwards theory [62] and stress-strain scaling, of the form:

$$\sigma_y \approx \frac{40k_bT}{V_{rod}}(\phi-\phi^*)^{3/2},$$ ....(7)

and, therefore, calculated a storage modulus that agreed reasonably with their data:

$$G' \approx \frac{\sigma_y}{\varepsilon} \approx \frac{40k_bT}{D_{eff}^3}(\phi-\phi^*)^2,$$ ....(8)

where the quantity $40k_bT$ is the nanotube-nanotube bond energy [63], ϕ is the volume fraction, ϕ^* is the percolation volume fraction, V_{rod} is the volume of the rod and surface coating, and D_{eff} is the rotary diffusion coefficient from the theory of Doi and Edwards.

CNTs suspended in low molecular weight liquids show a negative primary normal stress difference similar to that observed in lyotropic rod-like liquid crystalline
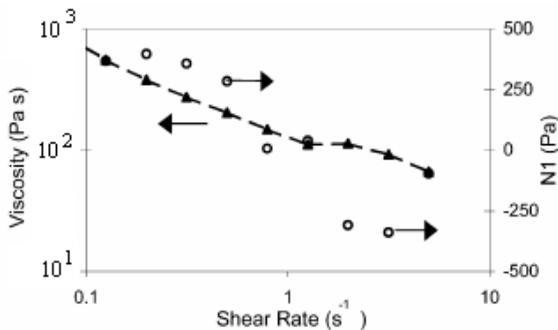

Figure 3.6: Viscosity and primary normal stress difference as a function of steady shear rate in a cone-plate rheometer for a 3.5 wt% single-walled nanotube suspension in 102% H_2SO_4. The authors draw the similarity to the triple zone LCP behavior [64].

polymers. Davis et al. [64] suspended single walled nanotubes in highly concentrated acids and observed a positive primary normal stress difference at low steady shear rates but became largely negative at higher shear rates. In figure 3.6 is shown the shear dependency of both viscosity and N_1 for CNTs suspended in super-sulfuric acid. The explanation for such behavior was adapted from discussions of N_1 behavior found in the liquid crystalline polymer (LCP) literature [65-68]. For an oversimplified explanation, the negative N_1 was attributed to the transition from the rod-like structure rotating or "tumbling" to fluctuating or "wagging" about an axis under appropriate stress. The N_1 values turned out to be positive as the rods or tubes aligned in the flow direction. Larson [4] provided an in depth general discussion of LCP rheology. Recent Stokesian dynamics simulations by Brady and Sierou [69] of low viscosity suspensions of concentrated low aspect ratio particles have shown large negative normal stresses under high deformation from interparticle lubrication, which could be the case for large aspect ratio fibers.

In general, CNFs are larger than CNTs and push the limits of nanoparticle definitions of size. A recent paper by Xu et al. [36] examined the effect of CNF dispersant method on rheological properties, where the dispersant method is defined as the treatment applied to the nanofibers by acid wash, sonication, or both, before mixing with a glycerol and water solution. The authors observed that $G' > G''$ for low frequency shear rates and that suspension viscosity increased with nanofiber loading. The development of a yield stress combined with the prior two effects led to the suggestion of a percolated CNF entanglement network. Xu et al. [36] reaffirmed the entanglement network from the observation of > 5 wt% CNF suspensions being too viscous for measurement. Yet, the suspensions tested shear- and strain-thinned, which was attributed to CNF alignment in the flow direction. Certainly alignment may occur, but an alternative may be from a lubrication effect of the small molecule solvent between the shearing (slip) planes of the CNF aggregates. Shear thinning diminished with decreasing particle concentration and aspect ratio, as previously noted by Brenner [70], and was caused by increased packing ability (see figure 3.1). In addition, all suspensions were non-thixotropic. Any breakdown of network structure due to alignment rapidly reformed because of the weak interactions between nanofiber agglomerates of non-Brownian nature.

4. RHEOLOGY OF NANOPARTICLE FILLED POLYMER LIQUIDS

4.1 Polymer Layered-Silicate Nanocomposites

The recent literature has examined the linear and non-linear viscoelastic properties of several clay-polymer combinations such as polyamides [71-77], polycarbonates [78-80], polyesters [81-84], polyolefin [85-95], polyvinyls [96-102], polystyrene [103-106], polystyrene-polyisoprene block copolymers [107-110], thermotropic liquid crystalline polymers [111, 112], elastomers [113, 114], other copolymers [115, 116], and biodegradable polymers [117, 118] among others [119-121]. The majority of rheological studies have focused on using the rheological properties to assess the state of nanoparticle dispersion. G' from oscillatory shear flow in the linear viscoelastic regime gives the most obvious indicator of nanoparticle dispersion,

because the composite will show a more solid-like response as the percolation network limit is reached. Transient shear experiments probe the microstructure development for the effects of inter-particle interactions. However, dispersion or exfoliation of anisotropic nanoclay platelets in polymer matrices depends on many variables such as composite preparation, molecular weight of the polymer, nanoclay surface treatment, nanoclay aspect ratio distribution, particle-particle interactions, and particle-polymer interactions, to name a few.

4.1.1 Dynamic Storage Modulus in Linear and Nonlinear Oscillatory Shear

In the linear viscoelastic region, dynamic moduli reflect the viscous and elastic character of complex liquids through the quantities of G'' and G' respectively. Most studies focus on the development of the elastic character, G', with the addition of nanoparticle filler because these studies are ultimately searching for enhanced mechanical properties. Typically, if the polymer is inherently viscous in nature, G'' exceeds G', but when rigid and semi-flexible solid particles are added G' approaches or exceeds G''. Although a change in loss modulus may occur, the change in storage modulus is typically much more sensitive. Therefore, much of the discussion of dynamic moduli pertains to the effects on G'.

The specific interest in G' is based on the development and extent of a low frequency plateau, or non-terminal slope, where essentially the elastic character is independent of angular frequency. In general, in the terminal region the storage and loss moduli scale as $G' \sim \omega^2$ and $G'' \sim \omega$. The formation of the low frequency plateau indicates gelation of the particles into mesostructural domains, which dictate the solid-like response. Whether the mesostructure exists as a percolated or critically entangled network or the solid-like response is due to geometric confinement is still under debate [85, 96, 107]. Rheology alone cannot determine the exact morphology, for example, between a soft-glass and gel [122]. Most rheological studies are complemented with electron imaging and light scattering to assess the degree of dispersion. The concentration at which this liquid-like to solid-like transition occurs depends upon the exfoliation or dispersion of the nanoclay within the polymer. Some of the factors dictating exfoliation observed in the literature are polymer matrix molecular weight, particle-particle interactions, particle-polymer affinity, platelet aspect ratio, etc. Associated with each of these factors are the effects of processing such as the method of nanocomposite formation (in-situ polymerization, solvent casted, melt blended) [see 2 for more examples], the surface treatment of the clays that allows for larger gallery spacing and functional sites for interaction, and the temperature of the test as some polymers are unstable at their melt temperature.

For conventionally filled composites, with greater than micron-sized particles, an increase in matrix molecular weight increases the magnitude of the low frequency storage modulus response at equal particulate concentrations greater than 30 weight percent. Nanocomposites require much lower amounts of filler to observe the same behavior. In a 3 wt% hydroxyl modified nanoclay and nylon 6 melt blended system, the terminal zone slope decreased with increasing molecular weight, as shown in figure 4.1 [74]. The authors believed that the increased shear from the longer and more
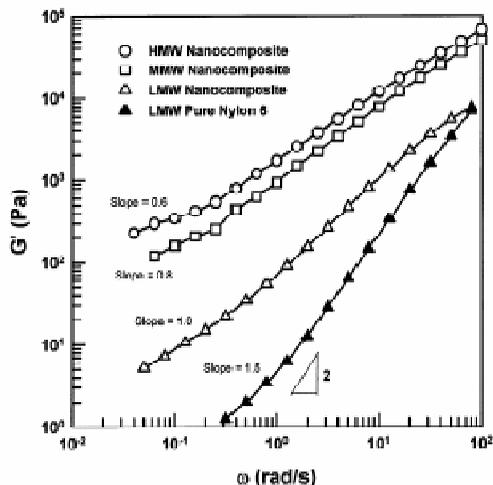
Figure 4.1: Role of polymer molecular weight on the G' of melt intercalated 3 wt% hydroxyl modified nanoclay/nylon 6 composites. T = 240C, HMW ~ 30K, MMW ~ 22K, LMW ~ 16K. [74].

entangled chains of the high molecular weight polymer aided the diffusion of chains into the platelet gaps, and exfoliated the nanoclays better than the lower molecular weights. Increased exfoliation led to a greater number of stronger particle-polymer interactions that served to increase G'.

For aggregated systems of particles at equal molecular weight and filler loading, the stacked platelets have a smaller aspect ratio and interact less with the polymer chains so that the terminal slope scales near to $G \sim \omega^2$. In-situ polymerization typically produces well-dispersed nanoclay composites, whereas melt blending leaves some intercalated stacks. Although studies of in-situ and melt-blended composites of the same molecular weight and polydispersity index and clay concentration have yet to be conducted, the end-tetherment of polyamide to the clay during polymerization has shown qualitatively a more pronounced elastic response than the melt blended counterparts [71, 73, 74, 77, 78].

The literature has instead focused on the effect of organic modifier of the clay surface on the strength of particle-particle and particle-polymer interactions. Lee and Han [78] investigated the effect of hydroxyl-modified nanoclay on the storage modulus of polycarbonates. The authors reported very little change in the low frequency behavior of unmodified clay, but a low frequency plateau in storage

modulus developed and broadened in frequency range for hydroxyl modified clay. The broadening of the plateau with clay concentration indicated the favorable interaction of PC and organically modified-nanoclay due to hydrogen bonding [78]. Yoon et al. [79] tested a myriad of clay surface treatments ranging from phenyl groups, long alkyl chains, and hydroxyl groups. However, direct comparison of the surface treatments was convoluted with significant molecular weight degradation of the PC phase. Even though the hydroxyl modified nanoclay preformed best in tensile tests, the molecular weight loss was greater than for some of the other composites tested, which showed higher G' plateaus in oscillatory shear [79]. Others observed degradation when dealing with polycondensates possessing carboxylic acid linkages [78, 80, 82]. A symptom of molecular weight degradation was manifested in dynamic moduli experiments when the low frequency storage modulus of the nanocomposites exceed that of the virgin polymer, but at higher frequencies the storage moduli of the nanocomposites are lower than those of the neat polymer, as shown in figure 4.2.

The cationic exchange of montmorillonite surface metals with organic salts lengthens inter-gallery spacing and provides better wetability between the polymer and clay. Sodium ions between galleries of fluoromica sheets were displaced by a long amine terminated polystyrene and a very short phenylethylamine to examine the effect
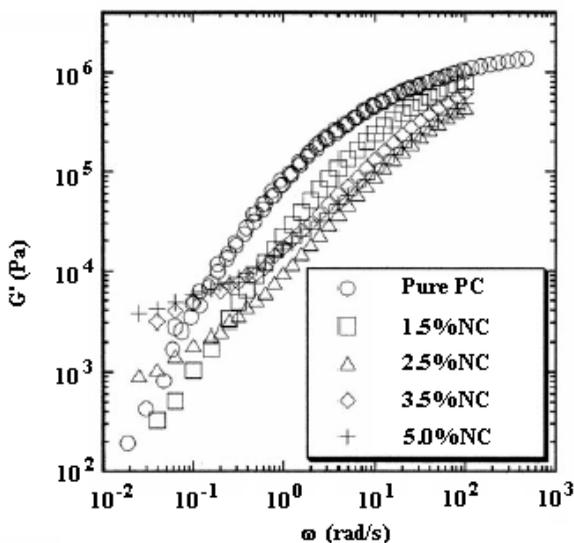

Figure 4.2: G' as a function of angular frequency for various PC and nanoclay (NC) composites as evidence of molecular weight loss, either by chain scission or depletion of continuous phase [80].

of modifier length on exfoliation in a linear polystyrene of narrow polydispersity [103]. The lengths of the modifiers differed by a factor of 50. The results show for equal loadings of silicate a plateau in G' in the long chain modified composite and G' behavior no different than that of the matrix for the shorter modifier chains. Electron imaging confirmed the significantly more exfoliated platelets for the long-chain-modified clay, indicating that large agglomerates do not significantly contribute to composite viscoelasticity at low concentrations.

Additional compatibility between phases aids in nanoclay dispersion and enhancement of rheological properties. Nanoclay/polypropylene composites typically involve a polypropylene grafted maleic anhydride plasticizer to compatiblize the hydrophilic clay surface and the hydrophobic polyolefin. As in most systems, nanoclay content increases the storage modulus of polypropylene melts at low frequency [87, 88, 91-93]. At high angular frequency, the inclusion of maleic anhydride produces a decrease in G' at some concentrations, due to the possibility of maleic anhydride's ability to degrade polypropylene [87, 123]. A recent study by Lertwimolnun and Vergens [93] showed the plasticizing effect of maleic anhydride as the elastic response was reduced, but the ternary mixture of PP-MAH-nanoclay showed a maximum in the low frequency storage modulus with increasing anhydride loading, as shown in figure
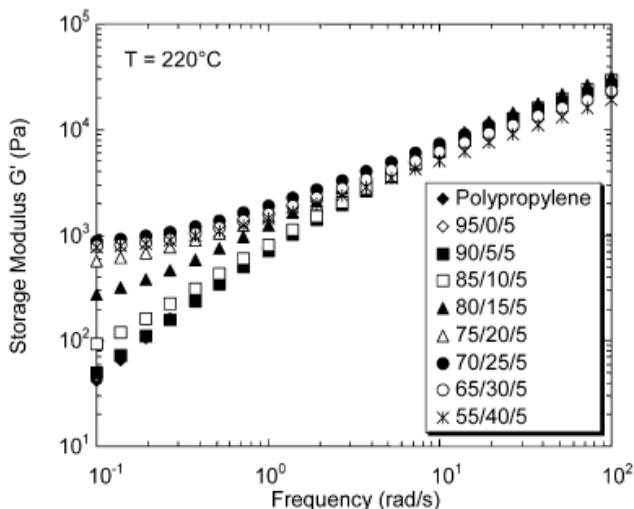

Figure 4.3: Effect of ternary compatibilizer on tallow modified nanoclay/PP composites, showing a maximum in G' with maleic anhydride concentration at low frequencies [93].

4.3. This maximum corresponded to the optimal amount of compatibilizer required for the best exfoliation of a long alkyl-modified nanoclay/PP composite [93]. Polyethylene-g-maleic anhydride nanoclay composites showed enhanced low frequency moduli over PE/clay composites at equal clay loadings [94, 105]. Similar results were obtained with polystyrene [105].

In terms of polyesters, maleic anhydride and pentaerythritol were used as compatibilizers in nanoclay/PET composites, but the effects of molecular weight degradation were too severe to draw any conclusions on the effect on G' [82]. A recent study by Wu et al. [83] examined the effect of a reactive epoxy on dispersing an organically modified nanoclay/PBT composite. At a constant nanoclay level the increase in epoxy compatibilizer increased the low frequency storage modulus response due to the greater number of PBT-epoxy-nanoclay interactions, which reduced the critical concentration for solid-like network formation compared to that of the PBT-nanoclay alone. Transesterification of the ester linkage of PBT was not observed by the authors.

Pre-alignment and pre-orientation of clay platelets to the flow direction before oscillatory shear decreases values of G' relative to those for the unoriented composites. The shear rate or strains required to align the platelets depends upon the numerous factors listed above. As the preshear rate increases subsequent oscillatory shear reveals a reduction in solid-like behavior (i.e. plateau in G'). A recent study on nanoclay/PBT composites showed the strength of particle-compatibilizer-polymer interactions dictated the magnitude of preshear needed for orientation [83]. The authors also showed (figure 4.4) the crossover frequency, where $G' = G''$, decreased with alignment reflecting the loss of elastic modulus due to orientation as the viscous polymer controls rheological response. Not only is the terminal zone slope eliminated with preshear, but the elastic response diminishes as the particles orient with surface normals perpendicular to the flow direction [83]. Lim and Park [105] examined on the effect of particle alignment on polystyrene and polyethylene composites. Total alignment of clay sheets was observed when all the viscoelastic properties reach steady state and the moduli reflected attributes of the neat polymer.

Studies outside the linear regime are not as common. Dynamic moduli that decrease with increasing strain amplitude in filled systems have been known for many years and generally the phenomenon is referred to as the Payne effect [124]. Sternstein and Zhu [96] developed a mesostructural mechanism from the observed Payne effect in nanoclay reinforced poly(vinyl acetate) and poly(vinyl alcohol) composites. The authors proposed the clay surfaces serve as contact points, and with the aid of Monte Carlo simulations [143] verified the "bridging' and "training" of polymer chains between and along clay surfaces that effectively increased the entanglement distribution. In another study, nanoclay-polycaprolactam end-tethered polymer-brushes strain-hardened after alignment to the direction of shear flow [72]. Strain hardening behavior was attributed to the pull and push of chains attached to the silicate surface from in situ polymerization [72]. The critical strain amplitude for the onset of strain hardening decreases with addition of silicate surfaces available for attachment. In other words, smaller strains were required to raise the viscosity of more densely entangled, tethered nanocomposites, similar to the jammed colloid of Cates et al. [126]
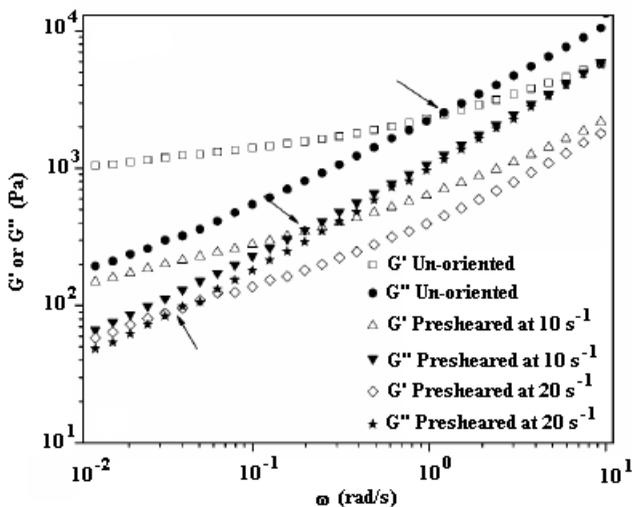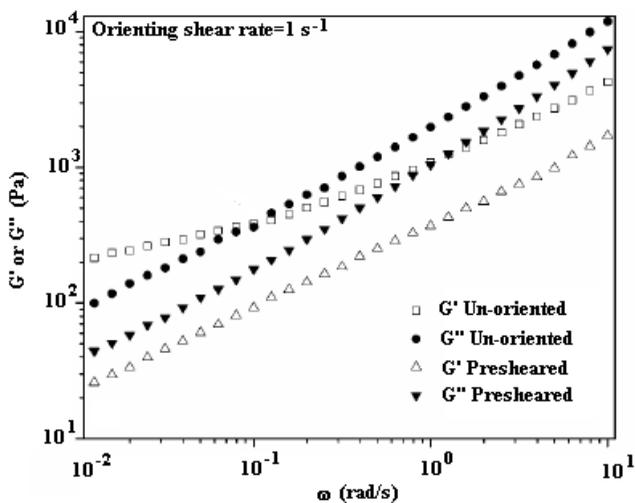
Figure 4.4: Effect of preshear on storage and loss moduli of (top) a 4 wt% hydroxyl modified nanoclay/PBT and (bot) 4 wt% hydroxyl-modified-nanoclay/ 4 wt% epoxy/ PBT composites [83].

4.1.2 Shear Thinning and Yield Stress Behavior

The addition of anisotropic nanoclay platelets enhances the low shear rate and low frequency viscosity of stable polymer matrices regardless of particle morphology. Subsequently, for a given concentration the degree of enhancement depends on the exfoliation with essential sub-factors such as surface treatment of the clay and the method of composite preparation. Typically as the clay concentration rises, the Newtonian plateau, if present in the neat polymer, gradually disappears until the percolation concentration is reached. At and beyond the percolation concentration, the composites exhibit strong non-Newtonian shear thinning at low angular frequencies and shear rates. Many authors reference the absence of Newtonian behavior as the presence of an apparent yield stress. Existence of a true yield stress may only be probed at very low controlled stresses, and some believe true yield is fiction as all materials flow given a large enough time scale [127]. Nonetheless, the apparent yield stress occurs simultaneously with the observations of meso-structural networks and solid-like behavior. Larger apparent yield stresses indicate stronger inter-particle and/or particle polymer interactions. Thus, electrostatic charge and particle-polymer affinity play significant roles in viscosity behavior, which are very much similar to the effects on storage modulus.

Interestingly, at high shear rate or frequency there is little increase in viscosity, if not a decrease as in cases of continuous phase depletion. At large deformations the network can no longer hold together and viscous polymer behavior dominates the response. The polymer chains then open and intercalate platelet layers simultaneously aligning them to flow. Alignment to flow has been checked by imposing steady shear for prescribed periods followed by dynamic oscillations, which show a decrease in the composite viscosity from the destruction of the network. Light scattering methods have verified the orientation of clay platelets to the shear flow direction [90].

Furthermore, the Cox-Merz rule is generally invalid for these nanocomposites. Briefly, the Cox-Merz rule empirically states the equivalence of complex and steady shear viscosities, $|\eta^*(\omega)| \approx \eta(\dot{\gamma})$ for $\omega = \dot{\gamma}$, and works well for many homopolymers. Typically, complex viscosity data are greater than steady shear data, indicating network destruction by steady deformation in the low shear region, $< 10^2 \text{ s}^{-1}$, and orientation of platelets in flow. Failure of the Cox-Merz rule is not unique to nanofilled materials, but has been observed in many conventionally filled polymer composites and liquid crystalline polymers among others.

In general, as molecular weight of the continuous phase increases shear thinning of the complex and shear viscosity become more pronounced. Fornes et al [74] examined the effects molecular weight on viscosity for a melt compounded nanoclay/nylon6 system. Figure 4.5 shows that although all neat resins exhibited Newtonian behavior, shear thinning increased with molecular weight. The shear thinning behavior was attributed to increased stress that the higher molecular weight polymer exerts on the platelets, which effectively peels the layers and allows intercalation of polymer into the galleries [74]. At high angular frequencies the composites of each molecular weight do not show a significant difference in shear thinning, because of platelet alignment. Tung and coworkers [77] drew rough
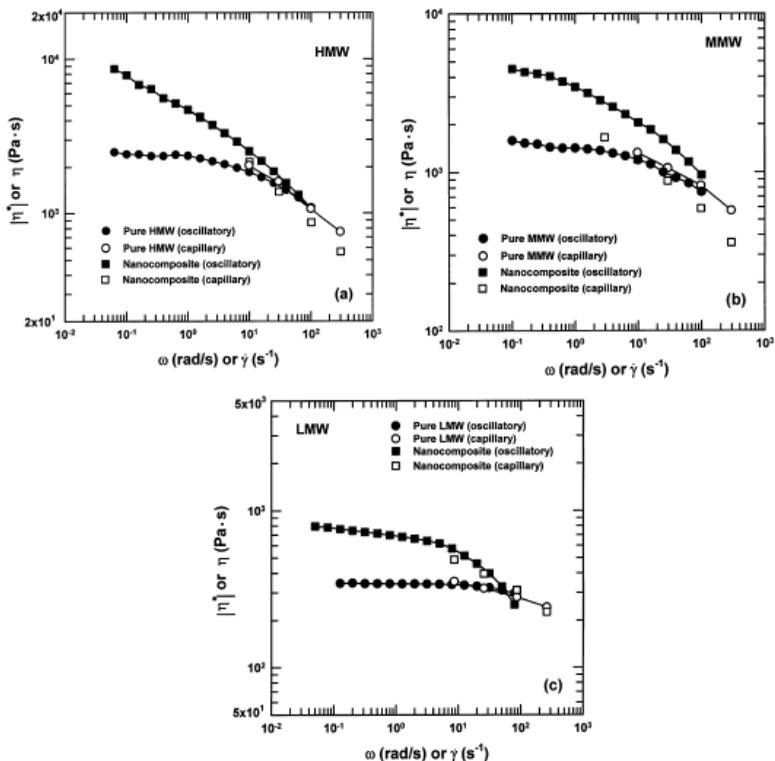
Figure 4.5 Failure of the Cox-Merz relation and the increased onset of shear thinning for three different molecular weights of nylon 6 and its nanocomposite of 3 wt% hydroxyl modified nanoclay. [74].

comparison between melt blended and in-situ polymerized nanoclay/nylon6 composite viscosities. In their study, at approximately equal clay concentrations the more exfoliated composite showed a greater steady shear viscosity, but equal shear thinning exponent. Many others have observed similar effects with different surface modifications [75, 78, 84, 91, 97, 119]. Lee and Han [78, 115] showed stronger particle-polymer interactions led to stronger shear thinning correlating to the presence of a stronger network. Hyun and coworkers [119] showed directly that an increase in clay modifier length produced a concomitant increase in exfoliation and complex viscosity in a PEO matrix.

Exceptions to the general observation of viscosity concomitantly increasing with filler loading do occur. Typically, these contrary observations occur in systems which degrade with filler addition. However, cases in which the molecular weight remains stable have been observed in capillary measurements of rubber-based nanocomposites and in dynamic measurements of soft-polymer particles suspended in the same linear polymer.

Sadhu and Bhowmick [114] observed that an apparent shear viscosity decrease may result from slip at the wall for nanoclay reinforced rubbers. The authors noted that the shear viscosity curve shifts downward to lower viscosities as the level of filler rose and decreases further when organically modified interacting clays were added. The processability of the rubber improved up to a critical concentration, at which particle agglomeration increased the shear viscosity (range $10-10^2$ s^{-1}). Figure 4.6 shows that the organically modified clay breaks up hydrogen bonds in the polar rubber and leads to a decrease in viscosity as rubber chains are more loosely bound in composites. Thus, Sadhu and Bhowmick [114] suggested the improved processability resulted from the nonpolar and unmodified nanoclays impeding the polar interactions between nitrile rubber chains. As an aside, the shear viscosity values increased for non-polar rubber/nanoclay composites.
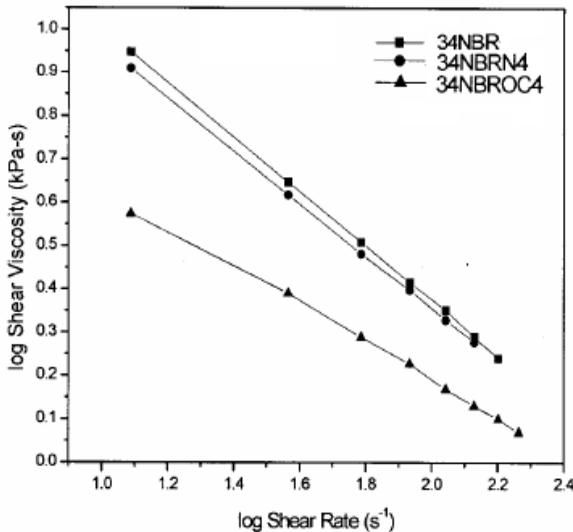

Figure 4.6: Decrease in apparent steady shear viscosity from capillary data on a acrylonitrile (34%) butadiene rubber (NBR) and its nanocomposite with unmodified (N4) and alkyl modified (OC4) nanoclays [114].
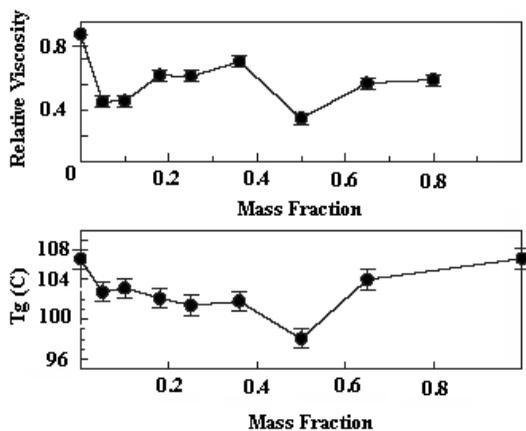
Figure 4.7: Relative viscosity and glass transition temperature as a function of filler mass fraction, for tightly crosslinked PS nanoparticles in a linear PS matrix [128]

Although collapsed or tightly crosslinked polymer particles may not be of high aspct ratio, these particles in suspension show viscosity decreases with increasing filler concentration. Mackay [128] has shown that in the absence of enthalpic restrictions dilute suspensions of well-dispersed crosslinked polystyrene nanospheres in a linear polystyrene matrix do not comply with Einstein predictions, i.e. relative viscosity decreases with filler concentration. A recent molecular dynamics simulation showed a qualitative agreement with the results of Mackay and coworkers [129]. The simulations showed that when the particles are smaller than the root-mean-squared radius of gyration, the particles act as a plasticizer to produce a viscosity decrease. Figure 4.7 shows the general trend of decreasing terminal viscosity with T_g as a function of tightly crosslinked PS nanoparticle concentration in linear PS. The zero shear or terminal viscosity was determined from the low frequency dynamic data. This genre of nanospheres increases the suspension free volume to decrease the composite glass transition.

In terms of yield stress in polymer layered silicate nanocomposites, Galgali and coworkers [85] observed the Newtonian behavior followed by a 3 order of magnitude decrease in viscosity within 500 Pa of shear stress of a relatively highly loaded (9 wt%) nanoclay/PP/maleic anhydride composite. The presence of a yield stress coincided with the low frequency nonterminal plateau in the storage modulus. The authors concluded that the solid-like or network response was a consequence of frictional drag imparted on the surfaces of the clay platelets. Yield stresses have been
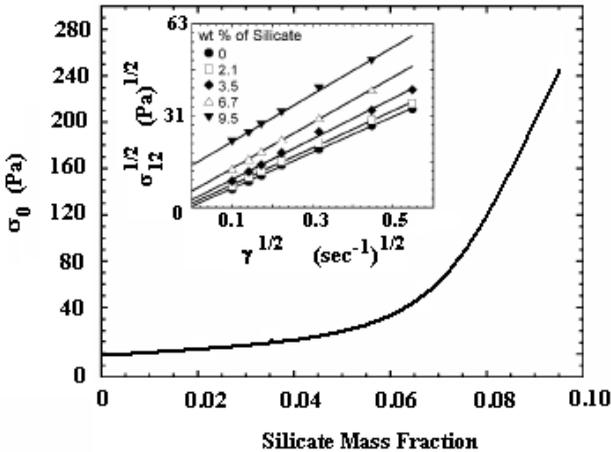
Figure 4.8: Yield stress as a function of clay loading and (inset) the correlation of experiment data to Casson's equation, for a PS-PI block copolymer. Yield stresses indicate the presence of solid-like behavior and some microstructural order [107].

determined from phenomenological equations fit to low shear rate data. Ren and Krishnamoorti [107] applied Casson's equation:

$$\sqrt{\sigma_{12}} = \sqrt{\sigma_0} + \beta\sqrt{\dot{\gamma}} , \qquad\qquad ....(9)$$

to low shear rate data of a polystyrene-polyisoprene/organoclay composite. Here, σ_{12} is the shear stress, σ_0 is the yield stress, and β is a fitting parameter. Casson's equation provided an excellent fit to their data, as shown in the inset in figure 4.8. The yield stress increased slowly at low clay concentration and then accelerated at high loadings indicating the existence of strong solid-like behavior and a network-type of mesostructure. Lertwimolnun and Vergnes [93] used a five parameter modified Careau-Yasuda model (equation 10) to determine the yield stress from dynamic frequency data for PP-g-maleic anhydride nanocomposites:

$$\eta(\omega) = \frac{\sigma_0}{\omega} + \eta_0[1 + (\lambda\omega)^a]^{(n-1)/a} , \qquad\qquad ....(10)$$

where η_0 is the zero shear viscosity, λ is a time constant, a is the Yasuda exponent, and n is the power law index. The presence of compatibilizer increased the yield behavior of the PP/nanoclay composite, although the intercalation distance between platelets did not significantly increase. Recently Zhong et al. [106] observed an

apparent yield stress in polystyrene nanocomposites from superimposable scaling ($\eta \sim \dot{\gamma}$) of capillary and parallel-plate steady shear viscosity data. Reported yield stresses in electro-rheological fluids, such as polyaniline polymers, are enhanced with the addition of modified nanoclays beyond the percolation limit [120, 121].

4.1.3 Thermal Effects on Viscoelasticity in Nanoclay Polymer Composites

Time-temperature superposition (TTS) is used to probe linear viscoelastic behavior at frequencies out of the typical range of oscillatory rheometers via shift factors relative to a given temperature. Thermorheologically simple polymer layered-silicate nanocomposites have been formed from several polymer-clay combinations [71, 87, 92, 101, 107]. In each case the shift factors are, to good approximation, independent of clay loading. A lack of temperature dependent relaxation of the silicate layers in the exfoliated composite leaves polymer chain relaxation to account for the superimposability of dynamic moduli [71]. Ren and co-workers [107] later added that intercalated chains between platelets relax on time scales much longer than those of the experiment and, therefore, show no contribution to TTS. This suggestion has led others to observe and recount the same non-Brownian effect from multilayered clay domains in polymer matrices [87, 92, 101].

TTS has not held for every polymer-nanoclay combination. The reasons for failure are different in each case. For a polystyrene-polyisoprene block copolymer above its order-disorder transition temperature, the moduli are superimposable. However, below this transition the changing matrix microstructure coupled with increasing agglomeration of particles with temperature lead to the failure of TTS at low frequencies [109]. Less exfoliated solvent casted PS/clay nanocomposites showed non-superimposable low frequency dynamic moduli, where the moduli of better dispersed in-situ polymerized composites proved superimposable, because of possible desorption of polystyrene chains from the clay surface as a function of temperature [106]. Gelfer et al. [97] proposed the formation of physical crosslinks between the clay surface treatment and the EVA chains, so that the polymer chains replace surfactant molecules on the clay surfaces. Yet, no spectroscopy was used to verify their hypothesis. In studies of PC/clay composites failure of TTS was proposed to be as a result of severe molecular weight degradation with increasing clay content and temperature dependent formation of a percolated network [80]. Furthermore, TTS failure was attributed to the formation of a temporarily hydrogen bonded network between polar clay surfactant and carbonyl oxygens in the PC backbone that created divergent dynamic moduli at low frequencies [78]. Interestingly, Lee and Han [78] showed unmodified nanoclay/PC composites followed TTS, which could be due to of the hydrodynamic constraints lengthening the relaxation time as explained by Ren and co-workers [107]. Comparing the organic modified and unmodified cases, the weight loss of surfactant and/or polymer as a function of temperature could lead to low frequency non-superimposability.
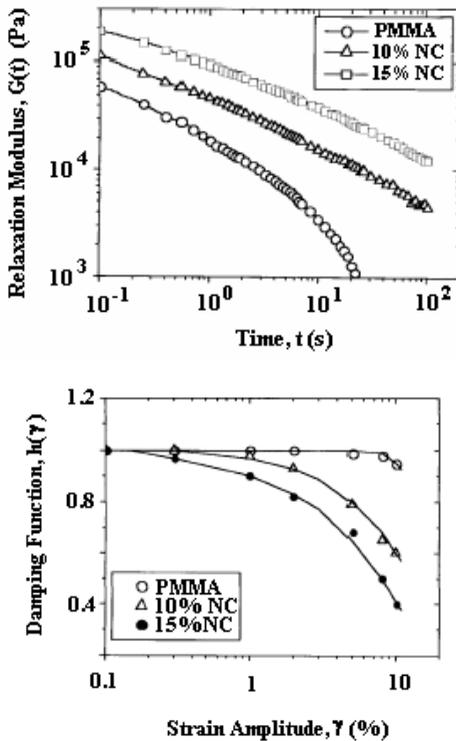
Figure 4.9: (Top) Low strain relaxation modulus $G(t)$ as a function of clay loading, line represents the fit to calculated relaxation spectra [122]. (Bottom) Characteristic damping function as a function of clay loading, line represents fit to PSM damping model [101].

4.1.4 Transient Rheology

Time-dependent rheology probes the transient effects of nanoclay loading on the temporal mesostructure development. The stress relaxation function from step strain and intermittent stress growth from the onset of steady shear shed insight into the relaxation processes and network formation behavior of the nanocomposites. In general, the curves of time dependent relaxation modulus, $G(t)$, increase and flatten in slope as the concentration of reasonably dispersed nanoclay increases [75, 91, 98, 101, 106, 110]. The upward shift and decreasing slope of $G(t)$ indicate longer relaxation times caused by the retardation of chain conformations from the presence of rigid two-

dimensional clay platelets. Figure 4.9 (top) shows the retardation of PMMA chains by nanoclay particles that slow the relaxation dynamics shown by an increasing shift in linear relaxation modulus and onset of nonlinear strain amplitude [101]. Zhong and coworkers [106] found that the linear relaxation modulus of a PS/nanoclay composite was independent of temperature, suggesting that the colloidal interactions between platelets dominated the Brownian motions of the polymer chains.

The stress relaxation function, $G(t,\gamma)$, is typically expressed as a product of separable functions of time, $G(t)$, and strain, $h(\gamma)$ [130]. The damping function, $h(\gamma)$, is generally a non-linear function of strain at high amplitudes. Figure 4.9 (bottom) and subsequent studies conducted on $h(\gamma)$ revealed much stronger damping behavior characterized by the onset of non-linear behavior at lower strain amplitudes as the clay concentration increased [98, 101, 110]. The strain induced alignment of clay stacks was alleged to lead to such non-linear behavior.

The transient reformation behavior of nanocomposite mesostructure is typically quantified through stress growth observations as a function of time. Flow reversal experiments investigate the effect of nanoclay content and surface modification on the magnitude of stress overshoot, or the strength of network interactions, and the recovery time, the kinetics of network reformation. As expected, the magnitude of the stress overshoot and the time for recovery of the initial overshoot increased with the nanoclay concentration, as shown in figure 4.10 [78, 83, 87, 88]. An increase in nanoclay content increased the recovery time of stress overshoot, indicating that upon
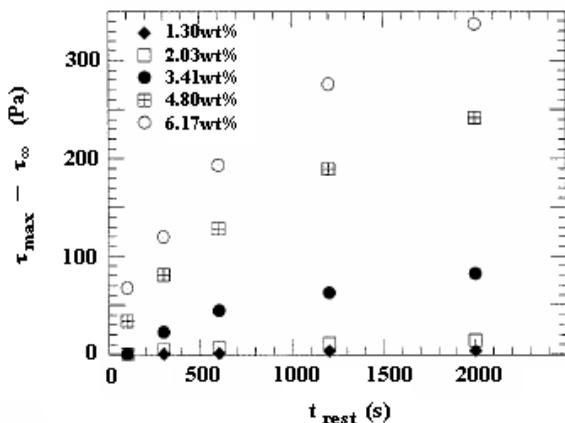

Figure 4.10: Magnitude of stress overshoot (represented as the difference between the peak stress and steady stress values) as functions of rest time (time allotment for structural reformation) and clay loading in PP/MAH matrix [87].

cessation of shear flow microstructural domains reformed and then strengthened depending on amount of clay-clay and clay-polymer interactions as well as time [87]. Surface modified organoclays that share favorable interactions with the matrix polymer also enhanced overshoot and recovery time more than unmodified nanoclay composites [78]. The stress overshoot in startup of shear depends on the distribution of particles and particle orientations that control particle-particle interactions [78, 87].

Solomon and coworkers scaled the stress overshoot with strain to probe the strain reliance of the particle-particle mesostructure and eliminate time-dependency (figure 4.11). The methods are similar to those used for evaluating the behaviors of LCPs except that the overshoots of Solomon's data did not scale in magnitude as they would for LCPs [4]. Low concentrations of intercalated clay in PP/MAH have shown no significant effect on stress overshoot indicating that the separation distance between dispersed stacks negated network formation. Furthermore, the recovery of stress for an unmodified clay/PC composite was found independent of deformation and rest time, while a possibly hydrogen bonded nanoclay/PC composite depended on adequate the time of recovery [78]. Wu et al. [83] found that a higher degree of flocculation between polymer and nanoclay prior to steady shear increased the magnitude of stress overshoot. Discussions in the recent literature have focused on colloidal reformation mechanisms as opposed to the Brownian motion of individual platelets [87]. Shear deformation is believed to break down and orient the intercalated clay stacks, which are too large for significant Brownian motion effects during flow. After cessation of
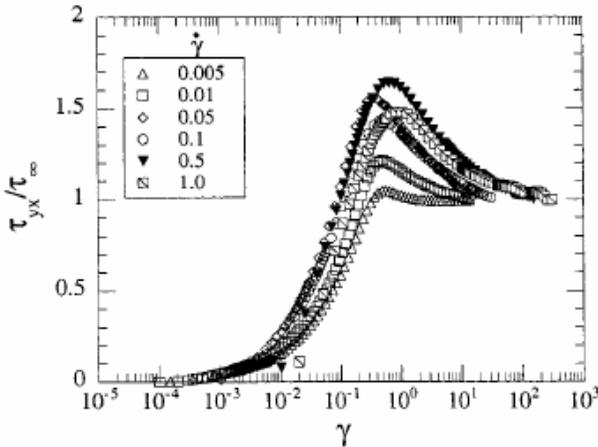

Figure 4.11: Stress-strain scaling of stress overshoot upon inception of steady shear flow for alkyl modified nanoclay/maleic anhydride/ PP composite. [87].

shear flow, the local particulate domains aggregate and reorganize through interparticle interactions, which rupture and align upon subsequent steady shear.

Rheopexy at very small shear rates has been observed for nanoclay filled polybutylene succinate [117]. The viscosity as a function of shear rate, between 10^{-3} and 10^{-2} s^{-1}, and nanoclay loading increased with time. The initial shear thickening, at steady shear, indicates the time scale of platelet alignment and orientation to the flow direction. Comparable to oscillatory shear, the particles dictate rheological response at low steady shear rate, but as the rate of deformation increases the polymer's contribution dominates and leads to shear thinning.

4.1.5 Normal Stresses and Flow Phenomena

A limited number of studies have examined the elastic behavior of layered-silicate nanocomposites. Current interest lies in understanding the significance of exfoliation as it applies to true elastic behavior. Yet, the scarcity of actual studies of N_1 results from suggestions that materials exhibiting large yield stresses complicate measurements of the normal stress [131, 132]. Therefore, the already difficult to measure normal stress depends on the distribution of platelets orientations that cause yield stresses among other factors.

In the current literature on the primary normal stress difference, the available studies have shown that nanoclay concentration has either no effect on N_1 or reduces N_1 relative to the neat polymer within an equal stress range. In both studies the shear viscosity did not depend on clay concentration at high shear rates, which has been shown to reduced elasticity in conventionally filled composites [99]. Additionally, matrix degradation with clay content was not observed, and polymer/clay compatibility produced well-dispersed intercalated composites. The influence of clay on N_1 may then depend on a relationship between the polymer and particle surface treatment. A block copolymer may not wet the particle surfaces sufficiently, because of the possible difference in block affinity for surface treatment, which creates weak polymer block-to-particle interactions and relatively little effect on elasticity. Therefore, in the case a strongly interacting polymer-particle systems, a decrease N_1 should be expected, but further studies are required to verify these conclusions.

However, the presence of nanoclay up to 9.5 wt% in a polystyrene-1,4 polyisoprene block copolymer showed no effect on the steady state values of N_1 [108]. Krishnamoorti et al. [108] ruled out the complications due to yield stress and confined local stress gradients that would produce slip between layers, because of the independence of viscosity and N_1 on nanoclay concentration. Instead the authors suggested that the absence of any influence of clay concentration was due to the alignment of the two-dimensional silicate layers under shear flow. It was reported that the orientation of the fillers in the flow direction eliminated surface to surface interactions between platelets and reduced the elastic energy [108].

Yet the observations of Gupta et al. [99] showed a decrease in N_1 with increasing clay content at high shear stresses on the order of 10^3 Pa (see figure 4.12). Figure 4.12 shows that increased nanoclay content restricted relaxation and reduced
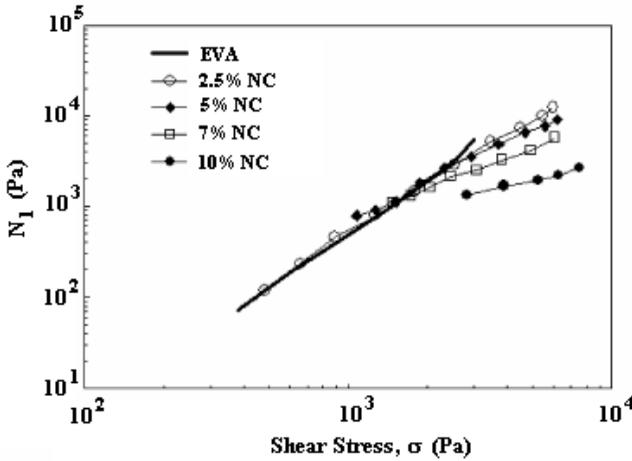
Figure 4.12: Primary normal stress difference as functions of shear stress and organoclay (NC) content in EVA nanocomposites [99].

the elasticity of the composite melt compared to the neat polymer. Thus, the reduced N_1 reflected the strong tendency of the exfoliated platelets to restrict the motion of polymer chains [99].

The phenomenon associated with the increase of the diameter of an extrudate as a melt leaves a capillary is known as die swell or extrudate swell, and defined as:

$$Die\ Swell\ \% = (D/D_o - 1) \times 100 , \qquad ....(11)$$

where D is the extrudate diameter and D_o is the die diameter. Consistent with the observations of decreasing N_1 with increasing clay content, the die swell of nanoclay composites was less than that of their neat polymers [106]. Die swell was also reduced in more exfoliated elastomeric polymers because of favorable polar interactions between clay surface treatment and acrylonitrile butadiene rubber [114]. Table 4.1 shows that for the case of nonpolar polybutadiene, die swell increased with clay loading and was attributed to poor particle-polymer interactions leading to particle agglomeration. For PS composites an increase in surface modified nanoclay concentration significantly reduces extrudate swell percentage. The overall reduction in die swell is a reflection of the retardation effect that the nanoclays have on the polymer relaxation time, much like the increase in time-dependent relaxation modulus.

In terms of flow stability, the critical shear rate for the onset of melt fracture was delayed up to 2-3 times the original threshold for an onium ion modified nanoclay

Matrix	Filler	Conc.	Die Swell (%)	Ref.
Polystyrene	None	-	57.0	106
	Alkyl modified NC	4 wt %	20.0	106
	Alkyl modified NC	9 wt %	4.0	106
Polybutadiene	None	-	52.9	114
	Unmodified NC	4 wt %	46.4	114
	Modified NC	4 wt %	59.7	114
Poly(styrene-butadiene) rubber	None	-	39.1	114
	Unmodified NC	4 wt %	38.4	114
	Modified NC	4 wt %	34.8	114
Poly(butadiene-acrylonitrile) rubber	None	-	62.2	114
	Unmod. NC	4 wt %	52.0	114
	mod. NC	4 wt %	49.1	114

Table 4.1: Effect of unmodified and surface treated (modified) nanoclay (NC) on the extrudate swell response from a capillary at constant shear rate given in the reference.

in linear low density polyethylene (LLDPE) with a large reduction in extrusion pressure [95]. Figure 4.13 shows the critical shear rate for the onset of gross melt fracture for a PP melt was delayed up to 170% the original shear rate when melt blended with 0.5wt% nanoclay. A combination of nanoclay with a fluoropolymer, known to be a processing aid, postponed critical shear for appearance of sharkskin to 10 times the critical value of neat LLDPE [95]. Interestingly the authors observed no or little change in critical shear rate for unmodified clays at equal concentrations as the modified nanoclays.

4.1.6 Extensional Rheology

Most rheological studies have focused on the effect of nanoclay concentration on the time-dependent uniaxial elongation viscosity expressed in units of time or Hencky strain [86, 99, 101, 102]. Predictions from linear viscoelasticity indicated that the extensional viscosity curve at low extension rates was equal to 3 times the zero shear viscosity, frequently called Trouton's ratio. Some studies have reported that this
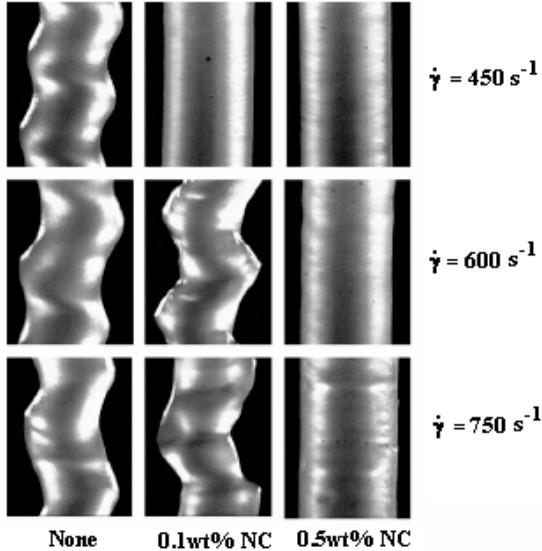
Figure 4.13: Suppression of critical shear rate for the onset of melt fracture for a pure PP melt, a 0.1 wt% and 0.5 wt% onium ion modified nanoclay/PP composite [95].

ratio holds for nanoclay composites in cases where a near steady state extensional viscosity is observed [101]. Others attributed the failure of Trouton's ratio to different mechanisms of mesostructural formation in shear compared to uniaxial elongation [86, 99]. No matter the system, the onset of strain hardening is always increased with the addition of nanoclay compared to the neat polymer. To draw an analogy, pure polyethylenes, with varying degrees of long chain branching, showed increases in strain hardening with the addition of polymer chain entanglements [133]. Thus, the presence of clay in the polymer matrix may create more entanglements or stronger polymer-clay networks that resist extensional deformation.

Early literature suggested the clays took a house of cards structure in an intercalated PP composite [86]. The card house reflected the flocculated edge to face colloidal interactions between the clay layers, which may have been a result of the presence of small amounts of maleic anhydride [86]. A shift in polarity of the suspending medium results in a change of interaction between the clay platelets, from face-face to edge-face attractions [1]. Yet, Okamoto and coauthors [86], by transmission electron microscopy (TEM) imaging, revealed platelets arranged with faces normal to the flow direction after deformation and not as a function of
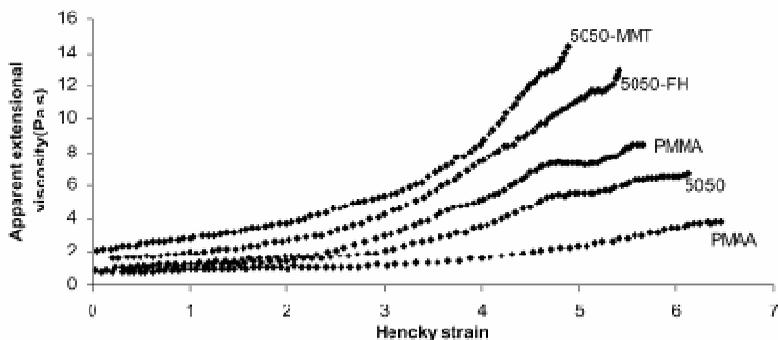
Figure 4.14: Extensional viscosity as a function of Hencky strain for 8wt% nanoclay (MMT) and fluorohectorite (FH) suspensions in a 50/50 copolymer of PMMA and PMAA [102]. In terms of size: FH >> MMT.

deformation time. Thus, localized stress variations between intercalated sheets may have created forces insufficient to induce alignment of all platelets in the flow direction.

More recent extensional viscosity studies have shown that the platelets align in the flow direction [102, 134]. Electrospun unmodified montmorillonite nanoclay and poly(MMA-co-MAA) copolymer composites showed (figure 4.14) a greater degree of strain hardening than larger sized particle composites and neat copolymer [102]. The increased strain hardening aided the formation of finer filaments of less than 500 nm in diameter [102]. Such a thin and uniform fiber could have only been produced from clay platelets aligning to the flow direction, because the length scale of a single platelet is of the diameter order of magnitude. Alignment of the platelets in the flow direction has been considered critical for stable fiber formation of nanocomposites [134]. The authors observed that less exfoliated larger platelets, which produced less uniform "drops" of large agglomerates still aligned in the flow direction. TEM analysis confirmed the exfoliated and aligned nanoclay structure. TEM and WAXD experiments on drawn polypropylene nanocomposites have verified the orientation of clay platelets in the flow direction [89, 92].

Gupta et al. [99] observed that although the onset of strain hardening was increased by the addition of nanoclay, at large Hencky strains the viscosity of the composites was less than that of the neat EVA matrix. The behavior, as shown in figure 4.15, suggested a competition between polymer-polymer and polymer particle interactions; such that the entanglement density created by the filler is reduced leading to lower stress. However, the possibility of colloidal interactions for well-exfoliated platelets cannot be eliminated. High extension rates geometrically bring clay platelets
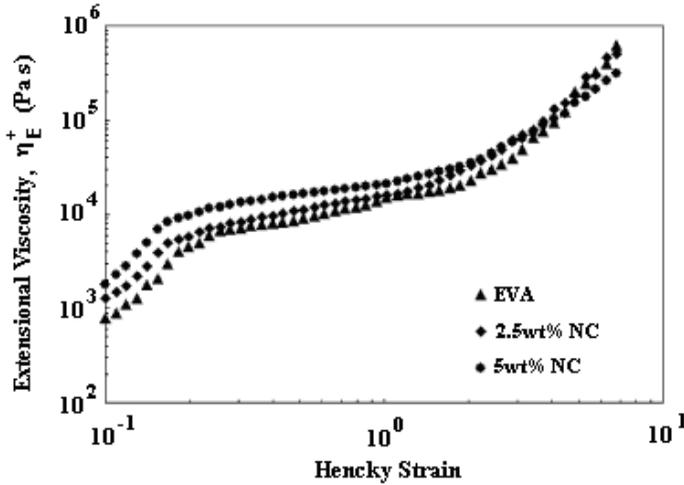
Figure 4.15: Extensional viscosity as function of Hencky strain and nanoclay loading for an alkyl ammonium modified clay melt blended with EVA [99].

into close contact, as the cross section is reduced with the square of the elongation rate. The decrease in plate separation gives rise to increased surface-to-surface attractions creating larger flocculated clay stacks [99]. The larger stacks of clay have trapped intercalated chains of EVA between the clay sheets, which effectively reduce the number of possible chain polymer chain entanglements necessary to produce further strain hardening [99]. TEM results verified the agglomeration of stacks after deformation.

4.2   Rheology of CNT and CNF Polymer Nanocomposites

To reap the rewards promised by increase electrical conductivity and increased elasticity in polymer-nanotube composites, the concentration of carbon nanotubes or nanofibers must exceed the percolation limit, which is exceptionally low compared to the silicates above. The critical volume fraction for the onset of percolation networking is inversely proportional to the cylinder aspect ratio for randomly dispersed particles [135]. As expected, enhancements of rheological properties occur at much lower concentrations of nanotubes than nanofibers because of the roughly order of magnitude difference in aspect ratios. However, these changes in rheological behavior depend on the polymer-nanocylinder network formation and not simple geometric confinement.

4.2.1   Dynamic Oscillatory Shear Measurements

Dispersions of CNTs in polycarbonate, polymethylmethacrylate, and polypropylene are among the few composites examined for rheological behavior. Despite the polymer matrix, increasing the concentration of nanotubes, either single or multi-walled, the complex viscosity increases. The degree of viscosity increase depends on the molecular weight of the polymer, the dispersion of the nanotubes, the isotropy of the tubes within the matrix, the nanotube aspect ratio distribution, and processing conditions. Therefore, the critical concentration for a percolated network structure depends on these factors as well.

A recent study examined the relationship of storage modulus to molecular weight of the polymer matrix at the same level of carbon nanotubes loading. For a 0.5 wt% CNT/PMMA nanocomposite, the higher molecular weight polymer showed a low frequency storage modulus plateau that was an order of magnitude greater than the lower molecular weight polymer, which deemed the rheological behavior as not dominated by the nanotube network [136]. The authors proposed the longer polymer chains restricted the motion of the tubes through the matrix, thus increasing storage modulus response and complex viscosity. The same authors reported the effect of nanotube dispersion or exfoliation within the polymer matrix. As the dispersion of the CNTs increased, the storage modulus curve shifted from terminal to non-terminal slopes and the low frequency modulus increased. Therefore, the percolation threshold for agglomerated systems increased to higher concentrations, which reflects the influence of aspect ratio. Agglomerated particles have smaller effective aspect ratios and, hence, the ability of these larger particles to percolate the matrix decreased. Figure 4.16 shows the rheological and electrical percolation threshold shown by the insulator-conductor transition as the conductivity increases 8 orders of magnitude over a 0.01 volume fraction increase and the shift toward solid-like behavior in the development of a 5 order of magnitude increase and non-terminal slope in G' from dynamic measurements.

Two studies indirectly showed the effect of longer processing time and higher temperature during processing. Potschke et al [137, 138] examined CNTs in different PC matrices. The authors observed a lower percolation threshold decrease to lower a concentration when the CNT and PC were allowed longer mixing time in a hotter extruder. Longer mixing time is traditionally believed to aid dispersion of particles, while the higher temperature could have stimulated chain motion to permeate and disperse the CNT domains.

Disentangled and agglomerated CNTs readily move with the matrix and diminish the shear thinning behavior of the suspensions. The observation that the onset of strong shear thinning of the complex viscosity with angular frequency as the concentration of nanotubes increases, denotes the percolation threshold. The material changes from liquid-like to solid-like in response. The shear thinning behavior of CNT/polypropylene composites was fitted to the Carreau model to quantify the degree of shear thinning with concentration [139]. Potschke et al. [138] concluded that the shear-thinning exponent decreased with CNT content and eventually became constant at higher loadings. However, at higher angular frequencies the rheological effects of

nanotube concentration were weakened. Du et al. [136] suggested that the CNTs did not affect the polymer chain dynamics, which was exemplified by the invariance of glass transition temperature with nanotube loading.

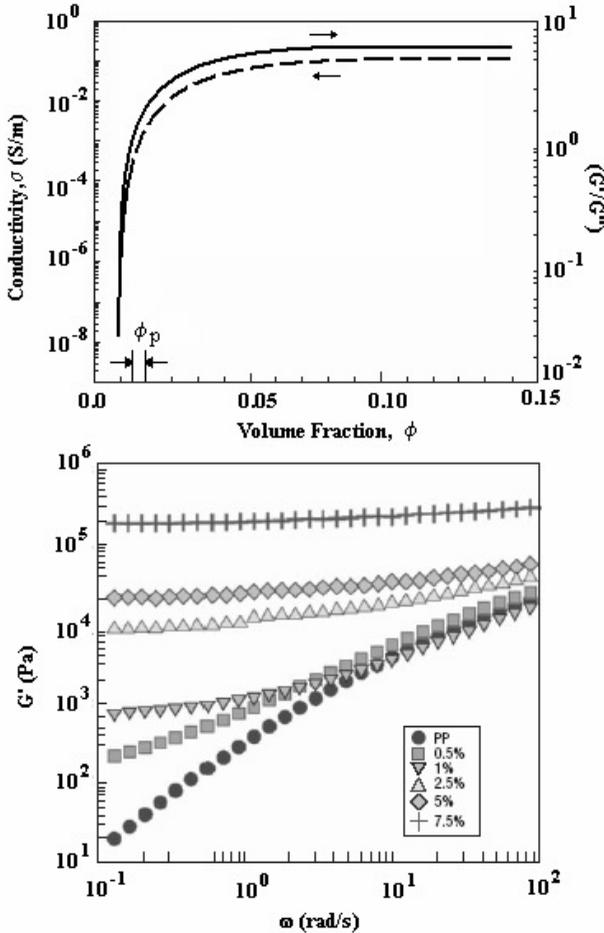**Figure 4.16:** (Top) Electrical conductivity and inverse loss tangent, expressed as G'/G'', as a function of CNT volume fraction in a PP matrix. (Bottom) G' as a function of angular frequency and CNT loading (vol%) melt blended with PP [139].

Dynamic shear provides a valuable insight into the relationship between rheological and electrical percolation. Less dense nanotube networks are not effective conductors of electricity, yet on average only one third of nanotubes are metallic. Therefore, electrical percolation thresholds require slightly larger amounts of nanotubes than rheological limits to ensure conductive contacts permeate [156]. Even though, for some matrices the electrical and rheological limits are nearly equivalent [137, 139].

The rheological attributes of CNF suspensions in polymer melts are essential by the same as CNT suspensions, except the phenomena indicating network formation occur at higher concentrations. Potschke et al. [138] reported a percolation concentration of CNT in a PC matrix an order of magnitude lower than the concentration required to form a network of CNFs in PP [140]. The rotations of short CNF were restricted by nearest neighbor interactions, because as the length of the fibers decrease the likelihood of fiber-fiber entanglements also declines [141]. Although solid-like behavior is observed in short and long CNF suspensions, the concentration for a critical network structure decreases with increasing length. The non-terminal slopes of storage modulus with angular frequency and the development of stronger shear thinning elucidate these observations expected from the close similarity to CNT suspensions.

Identification of the percolation limit is not always obvious from complex viscosity data, such as in cases where the matrix possesses an inherent microstructure. A comparison of complex and steady viscosities showed that the Cox-Merz rule is not applicable to system of thermotropic liquid crystalline polymer (TLCP) and CNF [142]. The isotropic ordering of liquid crystalline domains eliminated the low frequency Newtonian plateau, making the percolation threshold not as obvious from viscosity data alone. Therefore, the authors believed that the transition of the composite from originally viscously dominated, $G'' > G'$, liquid-like behavior to elastically dominated, $G'' < G'$, solid-like behavior with increasing concentration of CNFs marked a clearer network formation limit.

4.2.2   Normal Stress Difference and Elastic Effects

Studies of normal stress differences of CNT composites are rare, but the understanding is essential for processing applications. The sign of the primary normal stress difference appears to depend on the percolation concentration. From parallel plate steady shear experiments, Kharchenko et al. [139] determined the primary normal stress difference decreased with increasing nanotube loading shown in figure 4.17 (note this plot is $\Delta N = N_1\text{-}N_2$ vs. shear rate). Not only did N_1 decrease, it also became largely negative as the percolation concentration was exceeded. Typically, highly entangled polymer melts under shear exert a force against the plates that pushes them apart, creating a positive normal force. Cone and plate data revealed the primary normal stress difference was negative. The authors proposed that the large and negative N_1 was a consequence of the deformation of the percolated nanotube network
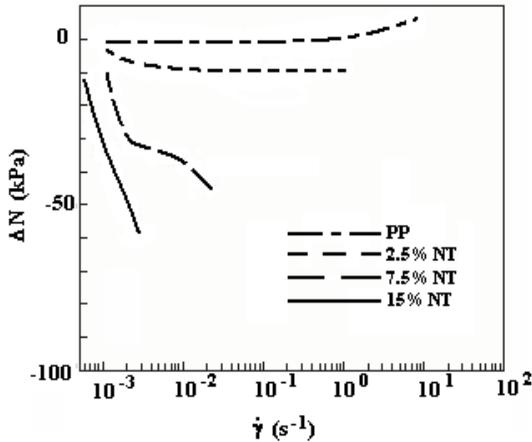
Figure 4.17: Negative normal stress difference from parallel plate rheometry ($\Delta N = N_1 - N_2$, where N_1 was deemed the more negative quantity) as a function of nanotube (NT) loading melt blended with PP [139].

by simultaneous stretching in the flow direction and compression in the direction normal to flow. These actions could be coupled to the elasticity of the nanotube cylinders, which may distort the flow streamlines similar to simulations of flexible fiber suspensions that were also shown to exert a negative normal stress difference [143].

A result of a negative normal stress difference may be the suppression of die swell behavior. Polyolefin melts, among others, show a post die expansion of the extrudate diameters that can range between 2-6 times the die diameter depending on molecular weight and extrusion rate. The addition of 2.5 vol % CNTs, a concentration above percolation, to a PP matrix showed a dramatic reduction in diameter compared to pure PP from the same die [139]. The authors also noted that CNT addition prevented shape distortion and the extrudate diameter was smaller than the die. The reduction of die swell has been observed for other systems such as polymer layered-silicate nanocomposites.

5. CONSTITUTIVE THEORIES FOR NANOPARTICLE FILLED POLYMER MELTS

5.1 Rheology and Structure

In this section we address whether fluids (primarily polymer melts) containing nano-particles require any special considerations concerning their rheology. Before one can model their rheology, it is necessary to have knowledge of their structure. We have seen that there is a plateau in G' at low frequencies similar to materials with yield stresses. We have also seen that peaks occur in the stress growth behavior and stress relaxation is retarded significantly. As we saw in section 2, dispersion or exfoliation of the individual platelets and particles is very difficult and, hence, the structural state of the system is unclear. As a result there are a number of questions which need to be answered. Is the rheology due to the effect of nano-size particles with high surface area? Is Brownian motion a significant factor in the process of relaxation? Is the structure possibly a percolated network in which recovery of structure is driven by thermodynamics? A knowledge of this structure is pertinent to not only developing constitutive equations but to understanding the state of the composite. In other words, the knowledge of the rheology may be an indicator of the state of the nano-composite (e.g. intercalated or exfoliated). In this section we review those rheological studies aimed at understanding what approach is required to model the rheology of nano-composites and studies concerned with modeling the rheology of these systems.

Solomon and coworkers [87] carried out an intensive rheological study involving both linear and non-linear shear behavior of polypropylene (PP) containing nano-clay particles. The particular system consisted of PP hybrid clay structures prepared using amine surfactants to promote intercalation. Above a concentration of 1.3 wt%, G' and G'' exhibited plateaus at low frequencies indicative of a viscoleastic solid or viscoleastic fluid with a characteristic relaxation time $> 10^2$ s, as no terminal region was observed for $\omega < 0.01$ s^{-1}. This was attributed to either the existence of a percolated network or rotational relaxation of anisometric clay platelets or platelet domains. Time-temperature superposition could be used to shift data obtained over a range of temperatures from 165 to 210 $^{\circ}$C to obtain a single master curve. The shift factor for the pure PP and composite were identical. This peculiar time-temperature superposition behavior was attributed to non-Brownian structure of the hybrid material [110].

To further explore the structure of these hybrids two additional non-linear rheological experiments were carried out by Solomon and coworkers [87]. Flow reversal experiments were carried out in which samples were sheared for 300 s at a shear rate of 0.1 s^{-1}. The flow was stopped and the sample was held quiescently for various times (0 to 2000 s) and then sheared in the reverse direction for 300 s and the same shear rate. The degree of stress overshoot was strongly dependent on the rest time which was believed by the authors to be a strong indication that the structure of the hybrid material evolved under quiescent conditions. The recovery could be due to either Brownian motion or strong thermodynamic interaction (i.e. aggregation). Reorganization due to Brownian motion can only be relevant if the characteristic dimension of the hybrid structure is sufficiently small. The crossover from Brownian

to non-Brownian behavior in a flowing suspension is controlled by a rotational Peclet number (or Weissenberg number):

$$Pe = \frac{\dot{\gamma}}{D_r} , \qquad\qquad ....(12)$$

where D_r is the rotational diffusion coefficient for a circular disk given by:

$$D_r = \frac{3k_bT}{4\eta_s d^3} , \qquad\qquad ....(13)$$

where η_s is the viscosity of the suspending medium. For the PP melt used by Solomon et al. (η_o = 2000 Pa s) it is estimated that d may be no larger than 300 nm for rotational relaxation to be due to Brownian motion. Individual clay particles are thought to have diameters in the range of 100 to 300 nm and, hence, if the particles were fully exfoliated and non-interacting, then Brownian motion could account for the recovery of structure.

The second set of experiments consisted of the stress growth behavior at the start up of shear flow. Solomon and coworkers [87] reported that the shear stresses scaled with strain. They interpreted this behavior to be characteristic of materials that possess no characteristic time scale such as thermotropic liquid crystalline polymers and non-Brownian suspensions of rods and disks [4]. However, for the scaling to be complete, the magnitude of the normalized stress must also scale with shear rate, and it did not as shown in figure 4.11. Entangled polymer melts also exhibit scaling of the peak stress with strain but not its magnitude [4]. Hence, it is unclear whether the interpretation of the results is correct.

From their work Solomon and coworkers [87] concluded that the structure most consistent with the experimental observations is one of non-Brownian particulate domains that are thermodynamically unstable and anisometric. The particulate domains were believed to consist of aggregates of multiple ordered platelets. Linear viscoelastic measurements alone could not be used to determine whether the platelet structure was networked or dispersed. Their interpretation was primarily based on their observation that the stress overshoot scaled with strain, which we have argued is not complete scaling as the magnitude of the normalized stress should also scale with shear strain. The linear and non-linear rheological properties were consistent with a hybrid structure of a weakly agglomerated network of multi-platelet particulate domains that was ruptured and reformed under flow and quiescent conditions.

For a suspension of nanotubes in a viscous solvent, the composite structure was that of a percolated network that heavily depended on particle-particle interactions. Kharchenko et al. [139] made similar calculations on the rotary diffusion coefficient to determine the dominating forces under flow. For a semi-concentrated suspension of rod-like particles [157]:

$$D_r = \frac{\beta k_b T \ln(a_r)}{3\pi\eta L^3 (nL^3)^2} \qquad\qquad ....(14)$$

where β is unity (from Doi and Edwards [157]), a_r is the nanotube aspect ratio, n is the number density of nanotubes, and L is the length of the nanotube. Kharchenko and coworkers determined that the Peclet number was of the order $10^{14} - 10^{16}$ and due to the large viscosity of the melt phase and relatively long nanotube length. Thus, for suspensions of multi-walled CNTs in viscous fluids the contribution of Brownian motion was negligible. Therefore, the rheological response of the percolated network structure was due to frictional and hydrodynamic forces.

5.2   Modeling the Rheology

Based on the discussions above, the polymer-nano-particle mixtures most frequently consist of non-Brownian particulate aggregates and on occasion single isolated particles (exfoliated). Various approaches have been proposed for describing the rheology of polymer-particle mixtures but with no specifications concerning particle size. Most of the models are based on network theory for the case of polymer-particle and polymer-polymer interactions but not for the agglomerated structures.

Ren and Krishnamoorti [110] proposed that the rheological behavior of polymer and clay nanocomposites at low shear rates resulted from the development of a three-dimensional percolated network meso-structure which is similar to the ideas of Solomon et al [87]. At higher shear rates the silicate layers align and steady state rheological properties approach those of the unfilled polymer [110]. Although it is unclear that the structure of polymer nano-clay composites would lead to rheological properties appropriately described by the K-BKZ constitutive equation, they evaluated the ability of this model to capture the rheological response of polystyrene-polyisoprene diblock copolymers and organically modified montmorillonite composites. They used step strain experiments to obtain the strain dependent relaxation modulus, $G(\gamma,t)$ as a function of time. They found that time-strain separability was valid for the composite materials but over a much smaller range of strain than that for the pure matrix. Furthermore, they found that a damping function of the form [158] (referred to as the PSM damping function):

$$h(\gamma) = \frac{1}{1 + \alpha\gamma^2} \qquad\qquad ....(15)$$

fit the nano-clay composite data well for clay concentrations from 0 to 9.5 wt%. The onset of strain for shear thinning decreased with increasing silicate loading for concentrations greater than 3.5 wt% and time-strain separability was valid only at much lower strains. They speculated that this behavior was due to the highly anisotropic silicate layers orienting when subjected to moderate and large strains. Furthermore, they speculated that this was the cause of shear thinning rather than confinement-induced shear thinning [159] or shear-induced disaggregation of the tactoids [108]. The disruption of the quiescent mesostructure at relatively modest

strains was surmised to result in the premature failure of time-strain separability for the higher silicate content nanocomposites.

According to the interpretation of Solomon and coworkers [87], the nanocomposite hybrid structure is one of a weakly agglomerated network of multi-platelet particulate domains that is ruptured and reformed under flow and quiescent conditions. When close-range filler interactions dominate, phenomenological models of filler cluster breakdown and re-agglomeration cluster networks have been proposed to describe some aspects of the resulting nonlinear viscoelastic behavior. These models were not aimed specifically at nano-sized particles nor was size a factor.

Leonov [146] proposed a continuum thermodynamic approach for the kinetics of floc evolution, which was successful in describing yielding, thixotropy, and frozen memory effects without using a yield criterion. Leonov proposed that the stress tensor was the sum of stresses due to matrix flow around flocs of particles and a stress in the flocs due to particle-particle interactions. The behavior of the matrix was modeled by the Leonov model [147]. A closed set of equations was obtained in terms of the deviatoric stress, strain rate, and Finger tensor. The particle mode was considered to be elastic leading to a general expression in terms of the configuration tensor and its invariants. Above a critical elastic energy stored in the flocs, or equivalently above a critical deformation of the flocs, the flocs started to rupture. The critical elastic energy was assumed to follow a Maxwell-type kinetic equation. Particle-particle interactions were considered in terms of attractive forces between particles leading to flocs behaving elastically before their rupture. Leonov and Simhabhatla [148] more recently considered strong polymer-particle interactions. The models were proposed to simulate the transient, yield, and thixotropic behavior of mixtures.

In another approach the filled system is assumed to consist of two independent networks. Doremus and Piau [149] assumed the matrix network is due to the segments of polymer chains between the particles. The second network is due to the polymer chains strongly absorbed on the particle surfaces. The kinetics of each network was described by an evolution equation proposed by Jamamoto [150]. The rates of formation and destruction of networks were taken as functions of the second invariant of the rate of deformation tensor. The rate of change of the configuration of the network was assumed to be proportional to the rate of deformation tensor and to the velocity gradient adjusted with a slip parameter. This gave rise to an expression for the stress tensor of a Gaussian network. The model predicts a yield stress value but not the stresses in the transient start up of flow. Inn and Wang [151] also used a double Yamamoto network model but assumed the additivity of the stresses due to entanglements and absorbed bonds. The functions describing the creation of the network segments were taken to be dependent on the volume fraction and on the ratio of the length of the polymer chain in the network to the diameter of the particle. The functions governing the rates of destruction of the networks were considered to increase with the length of the polymer chain in the network. There were no indications as to the ability of this approach to model the transient rheology of the composite system.

Havet and Isayev [152] employed a double network model also in which the network was created by the entangled polymer matrix and the absorbed polymer. Both networks were assumed to be described by the Giesekus constitutive relation [153]. They assumed that the total stress was the sum of contributions from the polymer and polymer-particle interactions but neglected the particle-particle interactions. The matrix rheology is assumed to be governed by the kinetics of creation and destruction of entanglements. The stress due to the polymer-filler interaction was considered to be due to the adsorption of the polymer onto the filler and to be proportional to the bridging density of the network created by the adsorbed polymer segments. During flow the polymer chains continuously absorb and desorb from the particle surfaces following an equilibrium process. The driving force for adsorption was expressed in terms of the Gibbs free energy which allowed one to calculate the rate constants for adsorption and desorption. Calculations for steady shear, stress growth, and stress relaxation were carried out as a function of relaxation time for the absorbed network and for various chain lengths between adsorbed sites. The predictions were qualitatively similar to the experimental behavior of polymers containing a well-dispersed filler.

In these analytical models, the dependence of the viscoelastic properties on filler size is not included. On the other hand, in many applications fillers with a size comparable to the characteristic length scale of the suspending medium (e.g. the radius of gyration of polymeric chains) are used. In such situations, additional physics may become important. The situation is complicated by the fact that in nanocomposites even at small filler volume fractions, a large surface area exists and most polymeric chains are close to the filler surface. Sarvestani and Picu [154] presented a conceptual
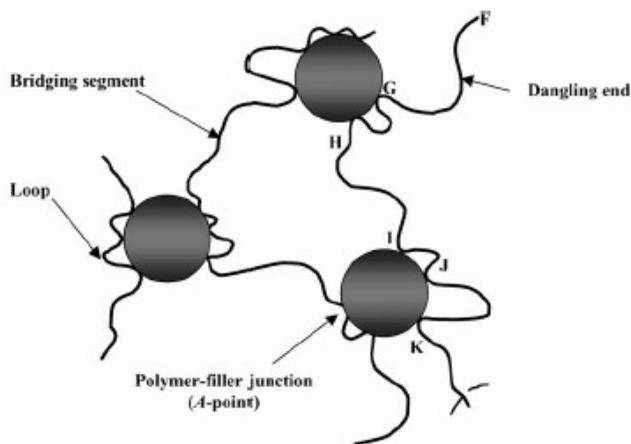

Figure 5.1 Schematic from Sarvestani and Picu [154]. The polymers bridge, loop, and dangle as they come in contact with and adsorb on to the nanoparticles.

model for the overall viscoelasticity of polymer nanocomposites with strong filler-polymer interactions. They considered non-agglomerated configurations in which rigid spherical nanoparticles with a diameter comparable to the radius of gyration of the polymer molecules were homogeneously dispersed in the polymeric matrix.

The proposed molecular structure is shown in figure 5.1. Three types of segments were identified: a bridging segment; a dangling end; a loop. The junctions were assumed to be reversible and their time evolution was due primarily to the applied deformation. The internal structure had a transient topology and its dynamics was controlled by the rate of the attachment and detachment process and depends on the applied deformation. The stress was assumed to be the superposition of contributions of the bridging and dangling segments. Network theory was used to describe the stress in the bridging segments, and the elastic dumbbell model was assumed to describe the stress contributions from dangling segments. The configuration distribution for the bridging segments was modified to include the rate of generation and destruction of bridging segments per unit volume. The configuration distribution function for the dangling chains was represented by a dumbbell model and considered one end of the chain fixed while the other end interacted with the matrix through a frictional contact. In order to obtain the configuration distribution functions the attachment/detachment dynamics of the chains from the particle surfaces were estimated using the approach of Chernyak and Leonov [155]. Calculations of G' and G'' showed that at low frequencies a solid-like plateau was predicted when the filler-polymer interaction was strong.

Even though typically contributions to the stress are assumed to come from both the matrix, the matrix particle and particle-particle interactions, Ren and Krishnamoorti [110] applied the K-BKZ constitutive equation to polystyrene-polyisoprene diblock copolymers and organically modified montmorillonite composites. The time dependence of the linear stress relaxation modulus, $G(t)$, was fit well by a sum of exponentials for both the matrix and the nano-composites, even for sample containing 9.5 wt% clay in which a tail in $G(t)$ was observed. The strain dependent part of the memory function was fit by the PSM damping function. At low shear rates, less than 0.2 s^{-1}, the K-BKZ model fit the shear stress growth data behavior well but failed at higher shear rates for the nanocomposites. The model fit the shear stress growth well at all shear rates for the matrix. The predicted steady shear viscosity agreed well with experimental data for shear rates up to 2.0 s^{-1} for both the matrix and the composites but under predicted the viscosity for higher shear rates. At all shear rates the model under predicted the primary normal stress difference, N_1, for both the matrix and the composites. Hence, the K-BKZ model using the linear $G(t)$ and the PSM damping function obtained from step strain experiments was inadequate for predicting the rheological data of the nano-composites as might be expected for fluids with potentially complex structure. The deviation of the model from the data was proposed to be due to the evolution of a mesoscale oriented structure at intermediate shear rates which was not covered by the damping function measurements. The failure of the K-BKZ model to predict N_1 suggested an inherent shortcoming of the model to describe the rheology of the nanocomposite system.

SUMMARY

In general, the addition of solid particles to low or high molecular weight liquids causes an increase in all viscoelastic parameters. As shown in this review, abnormalities such as strain thickening and large negative normal stress differences occur independently from liquid molecular weight. The tendency to compare nanocomposite to liquid crystalline polymers is cautioned, as such properties of stress scaling in start-up of steady shear flow do not apply. Other factors contribute against the general trend. Particle agglomeration or flocculation has the effect of artificially increasing particle concentration, and hence, the focus of most polymer nanocomposite literature lies on particle exfoliation. It is believed that exfoliated particles produce the largest increasing in mechanical properties, so that steric stabilizers, in the form of surface treatments, are added to reduce the van der Waals forces of attraction between platelets. One dimensional carbon nanotubes require the least amount of loading to reach a percolation threshold upon which the suspension possess characteristics more similar to a gel-like solid. The reformation of the mesostructural network after shear induced alignment of the large aspect ratio particles strictly depends on the thermodynamics of the composite system. Yet, the actual physics of mesostructural deformation in the nanocomposite melt is not completely understood, and many authors have attempted to describe the flow behavior through constitutive equations.

ACKNOWLEDGEMENTS

REFERENCES

1.   van Olphen, H, *Clay Colloid Chemistry*. Wiley & Sons, New York, (1977).

2.   Ray, S S and Okamoto, M, Polymer/layered silicate nanocomposites: a review from preparation to processing. Prog. Polym. Sci., 28 (2003) 1539-1641.

3.   Solomon, M J and Lu, Q, Rheology and dynamics of particles in viscoelastic media. Curr. Opin. Colloid & Inter. Sci., 6 (2001) 430-437.

4.   Larson, R G, *The Structure and Rheology of Complex Fluids,* Oxford University Press, New York (1999).

5.   Luckham, P F and Rossi, S, The colloidal and rheological properties of bentonite suspensions, Adv. Colloid & Interface Sci., 82 (1999) 43-92.

6.   Shenoy, A V, *Rheology of Filled Polymer Systems,* Kluwer Academic. London, (1999).

7.   Barnes, H A, Review of the rheology of filled viscoelastic systems, *Rheology Reviews*, The British Society of Rheology, (2003).

8.   Metzner, A B, Rheology of suspensions in polymeric liquids. J. Rheology, 29 (1985) 739-775.

9.   Krishnamoorti, R, Vaia, R A and Giannelis, E P, Structure and dynamics of polymer-layered silicate nanocomposites, Chem. Mater., 8 (1996) 1728-1734.

10. Krishnamoorti, R and Yurekli, K, Rheology of polymer layered silicate nanocomposites, Curr. Opin. Colloid & Inter. Sci., 6 (2001) 464-470.

11. Kaneto, K, Tsuruta, M, Sakai, G, Cho, W Y and Ando, Y, Electrical conductivities of multi-wall carbon nanotubes. Synthetic Met., 103 (1999) 2543-2546.

12. Krishnan, A, Dujardin, E, Ebbesen, T W, Yianilos, P.N and Treacy, M M J, Young's modulus of single-walled nanotubes, Phys. Rev. B, 58 (1998), 14013–14019.

13. Hilding, J, Grulke, E A, Zhang, G Z and Lockwood, F, Dispersion of carbon nanotubes in liquids, J. Dispersion Sci & Tech., 24 (2003) 1-41.

14. Pan, Z W, Xie, S S, Chang, B H, Wang, C Y, Lu, L, Liu, W, Zhou, W Y, Li, W Z, and Qian, L X, Very long carbon nanotubes, Nature (London)., 394 (6694) (1998) 631-632.

15. Iijima, S, Helical microtubes of graphitic carbon, Nature (London), 354 (6348) (1991) 56-58.

16. Li, Y L, Yu, Y D and Liang, Y A, A novel method for synthesis of carbon nanotubes: Low temp. solid pyrolysis, J. Mater. Res., 12, (1997) 1678-1680.

17. Lee, B O, Woo, W J, Song, H S, Park, H S, Hahm, H S, Wu, J P and Kim, M S, EMI shielding properties of carbon nanofiber filled poly(vinylidene fluoride) coating materials, J Ind. & Eng. Chem. (Korea) , 7 (5) (2001) 305-309.

18. Xu, J, Wang, Y, Koelling, K W and Bechtel, S E, Rheology of polystyrene/carbon nanofiber composites, ANTEC Soc. Plast. Eng. (2005) 1950.

19. Blumstein, A, Polymerization of adsorbed monolayers: II. Thermal degradation of the inserted polymers, J Polym Sci., A 3 (1965) 2665–2673.

20. Theng, B K G, *Formation and properties of clay–polymer complexes*, Elsevier, Amsterdam (1979).

21. Islam, M F, Rojas, E, Bergey, D M, Johnson, A T and Yodh, A G, High weight fraction surfactant solubilization of single-wall carbon nanotubes in water, Nano Letters, 3 (2003) 269-273.

22. Lozana, K, Gaspar-Rosas, A and Barrera, E V, Rheological examination of C_{60} in low-density solutions, Carbon, 40 (2002) 271-276.

23. Hirsch, A, Sagman, U and Wilson, S R, Use of buckysome or carbon nanotube for drug delivery, U.S. Pat. Appl. Publ. (2004), 25 pp., Cont.-in-part of U.S. Ser. No. 367,646.

24.   Venkatesan, N, Yoshimitsu, J, Ito, Y, Shibata, N and Takada, K, Liquid filled nanoparticles as a drug delivery tool for protein therapeutics, Biomaterials, 26(34) (2005) 7154-7163.

25.   Hu, J J and Zabinski, J S, Nanotribology and lubrication mechanisms of inorganic fullerene-like MoS2 nanoparticles investigated using lateral force microscopy (LFM), Tribology Letters, 18(2) (2005) 173-180.

26.   Ginzburg, B M, Shibaev, L A, Melenevskaja, E Y, Pozdnjakov, A O, Pozdnjakov, O F, Ugolkov, V L, Sidorovich, A V, Smirnov, A S and Leksovskii, A M, Thermal and tribological properties of fullerene-containing composite systems: Part 1. Thermal stability of fullerene-polymer systems, J. Macromolecular Science, Physics, B43(6) (2004) 1193-1230.

27.   Rapoport, L, Nepomnyashchy, O, Verdyan, A, Popovitz-Biro, R, Volovik, Y, Ittah, B and Tenne, R, Polymer nanocomposites with fullerene-like solid lubricant, Advanced Engineering Materials 6 (2004) 44-48.

28.   Harth, E, Van Horn, B, Lee, V Y, Germack, D S, Gonzales, C P, Miller, R D and Hawker, C J, A facile approach to architecturally defined nanoparticles via intramolecular chain collapse, J. Amer. Chem. Soc., 124 (2002) 8653-8660.

29.   Tenne, R, Inorganic nanotubes and fullerene-like materials, Chem. Eur. J. 8, 23, (2002) 5296-5304.

30.   Einstein, A, On the theory of brownian movement, Ann. Phys. (Leipz.), 19 (1906) 371–381.

31.   Batchelor, G K, The stress generated in a non-dilute suspension of elongated particles by pure straining motion, J Fluid Mech., 46 (1971) 813–829.

32.   Baker, F, The viscosity of cellulose nitrate solutions, J. Chem. Soc. Trans., 103 (1913) 1653-75.

33.   Krieger, I M and Dougherty, T J, A mechanism for non-Newtonian flow in suspensions of rigid spheres, Trans. Soc. Rheol., 3 (1959) 137-152.

34.   Tsai, S C, Botts, D and Plouff, J, Effects of particle properties on the rheology of concentrated non-colloidal suspensions, J. Rheol., 36 (1992) 1291-1305.

35.   Quemada, D, Rheology of concentrated disperse systems and minimum energy dissipation principle: I. Viscosity-concentration relationship. Rheol. Acta, 16 (1977) 82-94.

36.   Barnes H A, Hutton, J F and Walters, K, An Introduction to Rheology. Elsevier, Amsterdam, (1989).

37.   Xu, J, Chatterjee, S, Koelling, K W, Wang, Y and Bechtel, S E, Shear and extensional rheology of carbon nanofiber suspensions, Rheol. Acta, 44 (2005) 537-562.

38.	Kislenko, V N and Verlinskaya, R M, Rheological behavior of kaolin and montmorillonite suspensions at low concentrations, J. Colloid Interface Sci., 244 (2001) 405-409.

39.	Norrish, K, The swelling of montmorillonite: Discuss. Faraday Soc., 19 (1954) 120-134.

40.	Swartzen-Allen, S L and Matijevic, E, Surface and colloid chemistry of clays, Chem. Rev., 74 (1974) 385-400.

41.	Hunter, R J, *Foundations of Colloid Science,* vol. 1, Oxford Univ. Press, New York, (1986).

42.	Keren, R, Shainberg, I and Klein, E, Settling and flocculation value of sodium-montmorillonite particles in aqueous media, Soil Sci. Soc. Am. J., 56 (1988) 76.

43.	Zhong Y and Wang, S Q, Exfoliation and yield behavior in nanodispersions of organically modified montmorillonite clay, J. Rheology, 47 (2003) 483-495.

44.	Heller, H and Keren, R, Rheology of Na-rich montmorillonite suspension as affected by electrolyte concentration and shear rate, Clay & Clay Minerals, 49 (2001) 286-291.

45.	Bekkour, K, Leyama, M, Benchabane, A and Scrivener, O, Time-dependent rheological behavior of bentonite suspensions: An experimental study, J. Rheology, 49 (2005) 1329-1345.

46.	Miano, F and Rabaioli, M R, Rheological scaling of montmorillonite suspensions: the effect of electrolytes and polyelectrolytes, Colloids Surf. A. 84 (1994) 229.

47.	Rand, B, Pekenc, E, Goodwin, J W and Smith, R W, Investigation into the existence of edge—face coagulated structures in Na-montmorillonite suspensions, J. Chem. Soc. Faraday Trans 1, 76 (1980) 225.

48.	Pignon, F, Magnin, A and Piau, J-M, Thixotropic behavior of clay dispersions: Combinations of scattering and rheometric techniques, 42 (1998) 1349-1373.

49.	De Groot, J, Jon, V, Macosko, C W, Kume, T and Hashimoto, T, Flow induced anisotropic SALS in silica filled PDMS liquids, J. Colloid Interface Sci., 166 (1994) 404-413.

50.	Potanin, A A, On the mechanism of aggregation in the shear flow of suspensions, J. Colloid Interface Sci., 145 (1991) 140-157.

51.	Potanin, A A, On the computer simulation of the deformation and break-up of colloidal aggregates in shear flow, J. Colloid Interface Sci., 157 (1993) 399-410.

52.	Schott, H, Deflocculation of swelling clays by nonionic and anionic detergents. J. Colloid Interface Sci., 26 (1968) 133-139.

53. Zamam, A A and Delorme, N, Effect of polymer bridging on rheological properties of dispersions of charged silica particles in the presence of low-molecular-weight physically adsorbed pol(ethylene oxide), Rheologica Acta, 41 (2002) 408-417.

54. Heath, D and Tadros, T F, Influence of pH, electrolyte, and poly(vinyl alcohol) addition on the rheological characteristics of aqueous dispersions of sodium montmorillonite, J. Colloid Interf. Sci., 93 (1983) 307-319.

55. Brown, J M, Curliss, D and Vaia, R A, Thermoset-layered silicate nanocomposites: Quaternary ammonium montmorillonite with primary diamine cured epoxies, Chem. Mater., 12 (2000) 3376-3384.

56. Dean, D, Walker, R, Theodore, M, Hampton, E and Nyairo, E, Chemorheology and properties of epoxy/layered silicate nanocomposites, Polymer, 46 (2005) 3014-3021.

57. Le Pluart, L, Duchet, J, Sautereau, H, Halley, P and Gerard, J.-F, Rheological properties of organoclay suspensions in epoxy network precursors, Applied Clay Science, 25 (2004) 207-219.

58. Moraru, V N, Structure formation of alkylammonium montmorillonites in organic media, Applied Clay Science, 19 (2001) 11–26.

59. Hough L A, Islam M F, Janmey, P A and Yodh, A G, Viscoelasticity of single wall carbon nanotube suspensions, Physical Rev. Lett., 93 (2004) 168102-1-4.

60. Advani, S G and Zhihang, F, Effect of dispersion state on the rheology of multi-walled carbon nanotube suspensions in shear flow, AIP Conference Proceedings, 712 (2004) 1619-1623.

61. Gardel, M L, Shin, J H, MacKintosh, F C, Mahadevan, L, Matsudaira, P and Weitz, D A, Elastic behavior of cross-linked and bundled actin networks, Science, 304 (2004) 1301-1305.

62. Doi, M and Edwards, S F, *The Theory of Polymer Dynamics,* Clarendon, Oxford, (1992).

63. Girifalco, L A, Hodak, M, and Lee, R S, Carbon nanotubes, buckyballs, ropes, and a universal graphitic potential, Phys. Rev. B: Cond. Matter & Mater. Phys. 62 (2000) 13104-13110.

64. Davis, V A, Ericson, L M, Parra-Vasquez, A, Nicholas, G, Fan, H, Wang, Y, Prieto, V, Longoria, J A, Ramesh, S, Saini, R K, Kittrell, C, Billups, W E, Adams, W W, Hauge, R H, Smalley, R E and Pasquali, M, Phase Behavior and Rheology of SWNTs in Superacids, Macromolecules, 37 (2004) 154-160.

65. Marrucci, G and Maffetone, P L, Description of the liquid-crystalline phase of rodlike polymers at high shear rates, Macromolecules, 22 (1989) 4076-4082.

66. Larson, R G, Arrested tumbling in shearing flows of liquid-crystal polymers, Macromolecules, 23(17) (1990) 3983-3992.

67. Larson, R G and Doi, M, Mesoscopic domain theory for textured liquid crystalline polymers, J. Rheol., 35 (1991) 539-563.

68. Marrucci, G, Liquid crystallinity in polymers, VCH Publishers: New York, (1991) 395-421.

69. Sierou, A and Brady, J F, Rheology and microstructure in concentrated noncolloidal suspensions, J. Rheol., 46 (2002) 1031-1056.

70. Brenner, H, Rheology of a dilute suspension of brownian particles, Int. J. Multiphase Flow, 1 (1974) 195-341.

71. Krishnamoorti, R and Giannelis, E P, Rheology of end-tethered polymer layered silicate nanocomposites, Macromolecules, 30 (1997) 4097-4102.

72. Krishnamoorti, R and Giannelis, E P, Strain hardening in model polymer brushes under shear, Lagmuir, 17 (2001) 1448-1452.

73. Cho, J W and Paul, D R, Nylon 6 nanocomposites by melt compounding, Polymer, 42 (2001) 1083-1094.

74. Fornes, T D, Yoon, P J, Keskkula, H and Paul, D R, Nylon 6 nanocomposites: The effect of matrix molecular weight, Polymer, 42 (2001) 9929-9940.

75. Incarnato, L, Scarfato, P, Scatteia, L and Acierno, D, Rheological behavior of new melt compounded copolyamide nanocomposites, Polymer, 45 (2004) 3487-3496.

76. Aubry, T, Razafinimaro, T and Mederic, P, Rheological investigation of the melt state elastic and yield properties of a poly-amide-12 layered silicate nanocomposite, J. Rheol., 49 (2005) 425-440.

77. Tung, J, Gupta, R K, Simon, G P, Edward, G H and Bhattacharya, S N, Rheological and mechanical comparative study of in situ polymerized and melt blended nylon 6 nanocomposites, Polymer, 46 (2005) 10405-10418.

78. Lee, K M and Han, C D, Effect of hydrogen bonding on the rheology of polycarbonate/organoclay nanocomposites, Polymer, 44 (2003) 4573-4588.

79. Yoon, P J, Hunter, D L and Paul, D R, Polycarbonate nanocomposites. Part 2: Degradation and color formation, Polymer, 44 (2003) 5341-5354.

80. Hsieh, A J, Moy, P, Beyer, F L, Madison, P, Napadensky, E, Ren, J and Krishnamoorti, R, Mechanical response and rheological properties of polycarbonate layered silicate nanocomposites, Polym. Eng. & Sci., 44 (2004) 825-837.

81. Wagener, R and Reisinger, T J G, A rheological method to compare the degree of exfoliation of nanocomposites, Polymer, 44 (2003) 7513-7518.

82. Sanchez-Solis, A, Romero-Ibarra, I, Estrada, M R, Calderas, F and Manero, O, Mechanical and rheological studies on polyethylen terephthalate-montmorillonite nanocomposites, Eng. & Sci., 44 (2004) 1094-1102.

83. Wu, D, Zhou, C, Yu, W and Fan, X, Effect of flocculated structure on rheology of poly(butylenes terephthalate)/clay nanocomposites, J. Polym. Sci, Part B: Polym. Phys., 43 (2005) 2807-2818.

84. Scarfato, P, Scatteia, L, Costa, G and Acierno, D, Effect of the Organoclay structure on morphology and rheological response of PBT nanocomposites, Macromol. Symp., 228 (2005) 125-137.

85. Galgali, G, Ramesh, C and Lele, A, A rheological study on the kinetics of hybrid formation in polypropylene nanocomposites, Macromolecules, 34 (2001) 852-858.

86. Okamoto, M, Nam, P H, Maiti, P, Kotaka, T, Hasegawa, N and Usuki, A, A house of cards structure in polypropylene/clay nanocomposites under elongational flow, Nano Letters, 1 (2001) 295-298.

87. Solomon, M J, Almusallum, A S, Seefeldt, K F, Somwangthanaroj, A and Varadan, P, Rheology of polypropylene/clay hybrid materials, Macromolecules, 34 (2001) 1864-1872.

88. Li, J, Zhou, C, Wang, C and Zhao, D, Study on rheological behavior of polypropylene/clay nanocomposites, J. Appl. Polym. Sci., 89 (2003) 3609-3617.

89. Pavlikova, S, Thomann, R, Reichert, P, Mulhaupt, R, Marcincin, A and Borsig, E, Fiber spinning from poly(propylene)-organoclay nanocomposite, J. Appl. Polym. Sci., 89 (2003) 604-611.

90. Koo, C M, Kim, M J, Choi, M H, Ki, S O and Chung, I J, Mechanical and rheological properties of maleated polyproylene-layered silicate nanocomposites with different morphology, J. Appl. Polym. Sci., 88 (2003) 1526-1535.

91. Gu, S.Y, Ren, J and Wang, Q F, Rheology of poly(propylene)/clay nanocomposites, J. Appl. Poly. Sci., 91 (2004) 2427-2434.

92. Koo, C M, Kim, J H, Wang, K H and Chung, I J, Melt-extensional properties and orientation behaviors of polypropylene-layered silicate nanocomposites, J. Polym Sci. Part B: Polym. Phys., 43 (2005) 158-167.

93. Lertwimolnun, W and Vergens, B, Influence of compatibilizer and processing conditions on the dispersion of nanoclay in a polypropylene matrix, Polymer, 46 (2005) 3462-3471.

94. Lee, J A, Kontopoulou, M and Parent, J S, Time and shear dependent rheology of maleated polyethylene and its nanocomposites, Polymer, 45 (2005) 6595-6600.

95. Hatzikiriakos, S G, Rathod, N and Muliawan, E B, The effect of nanoclays on the processibility of polyolefins, Polym. Eng. Sci., 45 (2005) 1098.

96. Sternstein, S S and Zhu, A J, Reinforcement mechanism of nanofilled polymer melts as elucidated by nonlinear viscoelastic behavior, Macromolecules, 35 (2002) 7262-7273.

97. Gelfer, M, Song, H H, Liu, L, Avila-Orta, C, Yang, L, Si, M, Hsiao, B S, Chu, B, Rafailovich, M and Tsou, A H, Manipulating the microstructure and rheology in polymer-organoclay composites, Polym. Eng. Sci., 42 (2002) 42, 1841-1851.

98. Pasanovi-Zujo, V, Gupta, R K and Bhattacharya, S N, A constitutive analysis of extensional flow of EVA nanocomposites, Intern. Polym. Processing XIX, 4 (2004) 388-394.

99. Gupta, R K, Pasanovi-Zujo, V and Bhattacharya, S N, Shear and extensional rheology of EVA/layered silicate nanocomposites, J. Non-Newt. Fluid Mech, 128 (2005) 116-125.

100. Gelfer, M Y, Burger, C, Chu, B, Hsiao, B S, Drozdov, A D, Si, M, Rafailovich, M, Sauer, B B and Golman, J W, Relationships between structure and rheology in model nanocomposites of ethylene-vinyl-based copolymers and organoclays, Macromolecules, 38 (2005) 3765-3775.

101. Kotsilkova, R, Rheology-structure relationship of polymer/layered silicate hybrids, Mech. Time-Dependent Mater., 6 (2002) 283-300.

102. Wang, M, Hsieh, A J and Rutledge, G C, Electrospinning of poly(MMA-co-MAA) copolymers and their layered silicate nanocomposites for improved thermal properties, Polymer, 46 (2005) 3407-3418.

103. Hoffman, B, Dietrich, C, Thomann, R, Friedrich, C and Mulhaupt, R, Morphology and rheology of polystyrene nanocomposites based upon organoclay, Macomol. Rapid Commun., 21 (2000) 57-61.

104. Lim, Y T and Park, O O, Rheological evidence for the microstructure of intercalated polymer/layered silicate nanocomposites, Macomol. Rapid Commun., 21 (2000) 231-235.

105. Lim, Y Y and Park, O O, Phase morphology and rheological behavior of polymer/layered silicate nanocomposites, Rheol. Acta, 40 (2001) 220-229.

106. Zhong, Y, Zhu, Z and Wang, S Q, Synthesis and rheological properties of polystyrene/layered silicate nanocomposite, Polymer, 46 (2005) 3006-3013.

107. Ren, J, Silva, A S and Krishnamoorti, R, Linear viscoelasticity of disorder polystyrene-polyisoprene block copolymer based layered-silicate nanocomposites, Macromolecules, 33 (2000) 3739-3746.

108. Krishnamoorti, R, Ren, J and Silva, A S, Shear response of layered silicate nanocomposites, J. Chem. Phys., 114 (2001) 4968-4973.

109. Mitchell, C A and Krishnamoorti, R, Rheological properties of diblock copolymer/layered-silicate nanocomposites, J. Polym Sci. Part B: Polym. Phys., 40 (2002) 1343-1443.

110. Ren, J and Krishnamoorti, R, Nonlinear viscoelastic properties of layered-silicate-based intercalated nanocomposites, Macromolecules, 36 (2003) 4443-4451.

111. Lee, M W, Hu, X, Li, L, Yue, C Y, Tam, K C and Cheong, L Y, PP/LCP composites: effects of shear flwo, extensional flow, and nanofillers, Compos. Sci. & Tech., 63 (2003) 1921-1929.

112. Haung, W and Han, C D, Dispersion characteristics and rheology of organoclay nanocomposites based on a segmented main-chain liquid crystalline polymer having pendent pyridyl group, Macromolecules, 39 (2006) 257-267.

113. Jeon, H S, Rameshwaram, J K and Kim, G, Structure-property relationships in exfoliated polyisoprene/clay nanocomposites, J. Polm. Sci. Part B: Polym. Phys., 42 (2004) 1000-1009.

114. Sadhu, S and Bhowmick, A K, Unique rheological behavior of rubber based nanocomposites, J. Polym. Sci.: Part B Polym. Phys., 43 (2005) 1854-1864.

115. Lee, K M and Han, C D, Linear dynamic viscoelastic properties of functionalized block copolymer/organoclay nanocomposites, Macromolecules, 36 (2003) 804-815.

116. Chow, W S, Hohd Ishak, Z A and Karger-Koscis, J, Morphological and rheological properties of polyamide 6/poly(propylene)/organoclay nanocomposites, Macromol. Mater. & Eng., 290 (2005) 122-127.

117. Ray, S S, Okamoto, K and Okamoto, M, Structure-property relationship in biodegradable poly(butylene succinate)/layered silicate nanocomposites, Macromolecules, 36 (2003) 2355-2367.

118. Di, Y, Iannace, S, Di Maio, E and Nicolais, L, Poly(lactic acid)/organoclay nanocomposites: Thermal rheological properties and foam processing, J. Polym. Sci.: Part B Polym. Phys., 43 (2005) 689-698.

119. Hyun, Y H, Lim, S T, Choi, H J and Jhon, M S, Rheology of poly(ethylene oxide)/organoclay nanocomposites, Macromolecules, 34 (2001) 8084-8093.

120. Lim, Y T, Park, J H and Park, O O, Improved electrorheological effect in polyaniline nanocomposite suspensions, J. Colloid & Interface Sci., 245 (2002) 198-203.

121. Choi, H J, Kim, J W, Joo, J and Kim, B H, Synthesis and electrorheology of emulsion intercalated PANI-clay nanocomposite, Synthetic Metals, 121 (2001) 1325-1326.

122. Bonn, D, Kellay, H, Tanak, H, Wegdam, G and Meunier, J, Laponite: What is the Difference between a Gel and a Glass? Langmuir, 15 (1999) 7534-7536.

123. Ho, R M, Su, A C, Wu, C H and Chen, S I, Functionalization of polypropylene via melt mixing, Polymer, 34 (1993) 3264-3269.

124. Payne, A R J, The dynamic properties of carbon black-loaded natural rubber vulcanizates. Part I, Appl. Polym. Sci., 6 (1962) 57-63.

125. Cates, M E, Wittmer, J P, Bouchaud, J.-P and Claudin, P, Jamming, force chains, and fragile matter, Physical Rev. Lett., 81 (1998) 1841-1844.

126. Holmes, C B, Cates, M E, Fuchs, M and Sollich, P, Glass transitions and shear thickening suspension rheology, J. Rheology, 49 (2005) 237-269.

127. Barnes, H A, The yield stress—a review or 'παντα ρι'—everything flows? J. Non-Newt. Fluid Mech., 81 (1999) 133-178.

128. Mackay, M E, Dao, T T, Tuteja, A, Ho, D L, Van Horn, B, Kim, H .C and Hawker, C J, Nanoscale effects leading to non-Einstien-like decrease in viscosity, Nature Materials, 2 (2003) 762-766.

129. Karin, T, Daivis, P J, Ivanov, I and Bhattacharya, S N, Molecular-dynamics simulation of model polymer nanocomposite rheology and comparison with experiment, J. Chem. Phys., 123 (2005) 194905.

130. Ferry, J D, *Viscoelastic Properties of Polymers*, Wiley New York, (1980).

131. Tanaka, H and White J L, Experimental investigations of shear and elongational flow properties of polystyrene melts reinforced with calcium carbonate, titanium dioxide, and carbon black, Polym. Eng Sci., 20 (1980) 949.

132. Han, C D, *Multiphase Flow in Polymer Processing*, Academic, New York: (1981).

133. Bortner, M J, Doerpinghaus, P J and Baird, D G, Effects of sparse long chain branching on the spinning stability of LLDPEs, Int. Polym. Processing, 19(3) (2004) 236-243.

134. Fong, H, Liu, W, Wang, C S and Vaia, R A, Polymer, 43 (2002) 775-780.

135. Balberg, I, Recent developments in continuum percolation, Phil. Mag. B, 56 (1987) 991-1003.

136. Du, F, Scogna, R C, Zhou, W, Brand, S, Fischer, J E and Winey, K I, Nanotube networks in polymer nanocomposites: Rheology and electrical conductivity, Macromolecules, 37 (2004) 9048-9055.

137. Abel-Goad, M and Potschke, P, Rheological characterization of melt processed polycarbonate-multiwalled carbon nanotube composites, J. Non-Newt. Fluid Mech., 128 (2005) 2-6.

138. Potschke, P, Fornes, T D and Paul, D R, Rheological behavior of mutiwalled carbon nanotube/polycarbonate composites, Polymer, 43 (2002) 3247-3255.

139. Kharchenko, S B, Douglas, J F, Obrzut, J, Grulke, E A and Migler, K B, Flow-induced properties of nanotube-filled polymer materials, Nature Mater. 3 (2004) 564-568.

140. Loazano, K, Bonilla-Rios, J and Barrera, E V, A study on nanofiber-reinforced thermoplastic composites (II): Investigation of the mixing rheology and conduction properties, J. Appl. Polym. Sci., 80 (2001) 1162-1172.

141. Xu, J, Wang, Y, Koelling, K W and Bechtel, S E, Rheology of polystyrene/carbon nanofiber composites, ANTEC (2005) 1950-1954.

142. Lee, S, Kim, M S and Ogale, A A, Rheology of carbon nanofiber-modified thermotropic liquid crystalline polymers, ANTEC (2005) 1955-1957.

143. Becker, L E and Shelley, M J, Instability of elastic filaments in shear flow yields first-normal stress differences, Phys. Rev. Lett., 87 (2001) 198301.

144. Einstein, A, On the theory of brownian movement, Ann. Phys., 19 (1906) 371–381.

145. Ozmusul, M S, Picu, C R, Sternstien, S S and Kumar, S K, Lattice Monte Carlo simulations of chain conformations in polymer nanocomposites, Macromolecules, 38 (2005) 4495-4500.

146. Leonov, A I, On the rheology of filled polymers, J. Rheol., 34 (1990) 1039-1068.

147. Leonov, A I, On equilibrium thermodynamics and rheology of viscoelastic polymer media, Rheol. Acta, 29 (1976) 85-96.

148. Leonov, A I and Simhambhatla. M, On the rheological modeling of filled polymers with particle-matrix interactions, Rheol. Acta, 34 (1995) 329-338.

149. Doremus, P and Piau, J-M, Yield stress fluid: Structural model and transient shear flow behavior, J. Non-Newt. Fluid Mech., 39 (1991) 335-352.

150. Jamamoto, M, The viscolelastic properties of network structure. I. General formalism, J. Phys. Soc. Jap., 11 (1956) 413-421.

151. Inn, Y W and Wang, S Q, Transient network model for a multiphase polymeric fluid, Rheol. Acta, 32 (1993) 581-588.

152. Havet, G and Isayev, A I, A thermodynamic approach to the rheology of highly interactive filler-polymer mixtures: Part I – Theory, Rheol. Acta, 40 (2001) 570-581.

153. Giesekus, H, A simple constitutive equation for polymer fluids based on the concept of deformation dependent tensorial mobility, J. Non-Newt. Fluid Mech., 11 (1982) 69-109.

154. Sarvestani, A S and Picu, C R, Network model for the viscoelastic behavior of polymer nanocomposites, Polymer. 45 (2004) 7779-7790.

155. Chernyak, Y B and A I Leonov, On the theory of the adhesive friction of elastomers, Wear, 108 (1986) 105-138.

156. Powell, R.L. Rheology of suspensions of rod-like particles. J. Stat. Phys. 1991, 62, 1073-1094.

157. Doi, M. and Edwards, S.F. The Theory of Polymer Dynamics. Oxford Univ. Press. New York, 1986.

158. Papanastasiou, A C, Scriven, L E and Macoscko, C W, An integral constitutive equation for mixed flows: Viscoelastic characterization, J. Rheol., 27 (1983) 387-410.

159. Manias, E, Bitsanis, E, Hadziioannou, G and ten Brinke, G, On the nature of shear thinning in nanoscopically confined films, Europhys. Lett., 33 (1996) 371-376.